Regional assessment of daily reference evapotranspiration: can ground observations be replaced by blending ERA5-Land meteorological reanalysis and CM-SAF satellite-based radiation data?

A. Pelosi[1] and G.B. Chirico[2]

[1]Department of Civil Engineering (DICIV) - University of Salerno - Italy

[2]Department of Agricultural Sciences, University of Naples Federico II - Italy

Corresponding authors: A. Pelosi – apelosi@unisa.it

Highlights

- Shortwave radiation by CM-SAF outperforms ERA5-Land shortwave radiation
- ET_o is estimated by blending CM-SAF satellite-based radiation and ERA5-Land data
- ET_o computed by the blended dataset is as accurate as ET_o by interpolated ground data
- Blended datasets are good proxy for interpolated observations in data-sparse regions
- Shortwave radiation by CM-SAF outperforms spatially interpolated pyranometer data

This is a post-peer-review, pre-copyedit version of an article published in *Agricultural Water Management*.
The final authenticated version is available online at: *https://doi.org/10.1016/j.agwat.2021.107169*

Abstract

This study evaluates the accuracy of daily reference evapotranspiration (ET_o), computed according to the FAO Penman-Monteith equation by using a set of input weather variables obtained by blending ERA5-Land (ERA5L) reanalysis data with surface incoming solar radiation (R_s) provided by the instruments on board the Meteosat geostationary satellites, operationally delivered by the Satellite Applications Facility on Climate Monitoring (CM-SAF). Performance assessment was carried out in Sicily (southern Italy) by using data from 38 automatic ground weather stations (AWSs) for years 2003-2020. ERA5L and CM-SAF data were first downscaled and bias-corrected with a calibration dataset; ERA5L air temperature data were also downscaled by lapse-rate correction. ET_o estimates obtained with the blended ERA5L and CM-SAF validation dataset (ERA5L+CM-SAF) were compared with two other ET_o estimates respectively obtained by using ERA5L and interpolated ground weather data (IGD). Performance indicators of the IGD dataset were evaluated by recursively applying universal kriging or ordinary kriging to the observed weather data, according to a cross-validation procedure. R_s provided by CM-SAF outperformed R_s obtained by ground interpolation, thus confirming the convenience of using bias-corrected CM-SAF data even when ground observations are available in the study area. ET_o estimates with ERA5L+CM-SAF showed a normalized RMSE of 12%, outperforming ERA5L ET_o estimates while performing comparably to ET_o estimates obtained with the IGD dataset. The results suggested that the proposed blended dataset is a good proxy for interpolated ground weather observations in the assessment of ET_o at regional scale when weather measurements cannot be easily gathered or in data-sparse regions.

Keywords

Satellite-based models; reanalysis data; data-sparse regions; interpolated ground weather data; FAO Penman-Monteith ET_o; bias correction methods.

1. Introduction

Water resources management is one of the main global challenges of the 21st century, with many areas of the world likely to struggle in coping with demands for freshwater in the coming decades (Moore and Lobell, 2014). Agriculture is the economic sector with the largest consumptive water use and water withdrawal, accounting for almost 70% of global water withdrawn (Siebert et al., 2005). Assessing irrigation water use is thus fundamental for effectively planning the allocation of water resources in agriculture as well as for designing irrigation systems (Iglesias and Garrote, 2015), also in light of the United Nation’s (UN) 2030 Agenda for Sustainable Development (Llop and Ponce-Alifonso, 2016). The European Union, in compliance with European Water Framework Directive, has planned additional investments only for those irrigation infrastructures offering potential water savings of a minimum of between 5% and 25%, that should be verified by the implementation of reliable accounting systems of irrigation water use (European Parliament, 2013).

Quantitative assessment of irrigation water use at regional scale is generally based on crop-water-balance modeling (e.g., Allen, 2000; González-Dugo et al., 2009; Consoli and Vanella, 2014; Calera et al., 2017). Evapotranspiration is the key variable of the crop water budget, especially in those regions where rainfall and groundwater contribution are negligible in the irrigation season (Allen et al. 1998; Pereira et al., 2012; Pereira, 2017). Crop evapotranspiration is commonly estimated according to the FAO-56 procedure (Allen et al., 1998), as the product of a crop coefficient representing the crop state, and the grass reference evapotranspiration (ET_o) representing the evaporative demand of the atmosphere. The optimal method for estimating ET_o is the Penman-Monteith equation according to the FAO-56 formulation, provided that a complete set of meteorological data is available, including air temperature, wind speed, solar radiation, and relative humidity.

Ground weather stations, equipped with a complete and well-maintained set of reliable sensors, are generally sparse, even in developed countries. Time series of weather data collected by neighboring stations often present different temporal coverage and are not subjected to rigorous quality control procedures (Battisti et al., 2019). Data access is also a critical point: ground weather data are managed by regional and national services, which distribute data according to different policies. End-users may have access to these data after complex administrative procedures, with a significant latency.

In those regions where a ground set of weather data are available for the entire period of interest, a regional assessment of ET_o can be obtained by spatial interpolation (Lewis et al., 2014; String et al., 2017). The outcomes of spatial interpolations are subject not only to measurement errors but also to other uncertainties, such as uncertainty in the spatial structure of the interpolated field (Chirico et al., 2010), or the representativeness of the ground station site if the latter has not been selected according to adequate standards (e.g., WMO, 2018).

Methods other than the FAO Penman-Monteith have been proposed for computing ET_o with a reduced set of variables (Pereira, 2004; Paredes et al. 2020; Pelosi et al., 2020b), at the cost of an additional set of empirical parameters that must be calibrated with local data and, if possible, regionalized (Jung et al., 2016; Senatore et al., 2020). Such calibrated parameters are exposed to errors in the case of non-stationarities, as was observed in areas affected by significant climate change (Ren et al., 2016).

In the last two decades numerical weather prediction (NWP) models have provided additional sources of gridded weather data (Bauer et al., 2015). NWP models are mainly designed to forecast weather conditions and several studies have been conducted to exploit real-time NWP forecasts to support irrigation system operation and scheduling (e.g., Pelosi et al., 2016; Chirico et al., 2018; Medina et al., 2018; Longo-Minolo et al., 2020; Vanella et al., 2020). NWP models have also been implemented to reanalyze past weather conditions. Reanalysis data represent an efficient data source for planning and design studies applied to irrigation water management for two main reasons (Pelosi et al., 2020a): i) weather agencies distribute reanalysis data which are freely available on dedicated

This is a post-peer-review, pre-copyedit version of an article published in *Agricultural Water Management*.
The final authenticated version is available online at: *https://doi.org/10.1016/j.agwat.2021.107169*

web platforms, in a consistent spatial and temporal format; ii) end-users can easily process data also on regions extending across administrative boundaries, thus avoiding the burden of collecting and homogenizing weather station data from different data providers.

Several studies have evaluated ET_o prediction performance based on reanalysis data. The first used ERA-Interim data provided by the European Centre for Medium-Range Weather Forecasts (ECMWF) (e.g., Boulard et al., 2016; Paredes et al., 2018) and reanalysis data provided by the National Center for Environmental Prediction/National Center for Atmospheric Research (NCEP/NCAR) (e.g., Srivastava et al., 2015; Martins et al., 2017). In 2019, as part of the Copernicus Climate Change Service, the ECMWF released ERA5 reanalysis and ERA5-Land, produced by replaying the land component of the ERA5 climate reanalysis with a horizontal resolution of 9 km. Pelosi et al. (2020a) showed that the accuracy of daily ET_o predicted with ERA5-Land is comparable with that predicted by spatially interpolating ground weather data, but also pointed out that the incoming shortwave solar radiation reconstructed by ERA5-Land is the most prone to error among the weather variables involved in ET_o estimation.

Alternative sources for solar radiation data are provided by satellite-based products, such as those based on sensors mounted on geostationary satellites, like the Meteosat Visible and Infrared Imager (MVIRI) onboard the Meteosat First Generation and the Spinning Enhanced Visible and Infrared Imager (SEVIRI) on board the Meteosat Second Generation (MSG) satellites (Trigo et al., 2011; Urraca et al., 2017). Previous studies have evaluated the accuracy of ET_o obtained by coupling remotely sensed shortwave radiation with ground temperature observations (e.g., Cammalleri and Ciraolo, 2013; Cruz-Blanco et al., 2014). Paredes et al. (2021) evaluated the accuracy of ET_o estimates in Portugal obtained by coupling ground data with remote sensing radiation data provided by the Satellite Application Facility on Land Surface Analysis (LSA-SAF), as part of the European Organization for the Exploitation of Meteorological Satellites (EUMETSAT), based on SEVIRI images. LSA-SAF shortwave radiation outperformed ERA5 solar radiation, mainly due to the higher

This is a post-peer-review, pre-copyedit version of an article published in *Agricultural Water Management*.
The final authenticated version is available online at: *https://doi.org/10.1016/j.agwat.2021.107169*

spatial resolution (4 km for LSA-SAF and 31 km for ERA5). The accuracy of ET_o estimates was also slightly better with LSA-SAF solar radiation than with ERA5 solar radiation. However, LSA-SAF data were affected by many gaps in the time series, which made its operational use more difficult than ERA5.

The Satellite Application Facility on Climate Monitoring (CM-SAF) of EUMETSAT distributes surface incoming shortwave radiation (R_s) data from year 1983, produced by processing multispectral images of MVIRI and SEVIRI radiometers mounted on Meteosat satellites. The latest CM-SAF R_s products, based on SEVIRI radiometer mounted on MSG, are released operationally from year 2018 with a two-day delay. Urraca et al. (2017) verified the quality of CM-SAF Ra data, after validating it with 313 pyranometers distributed across all European countries, except Portugal and Italy.

The main motivation of this study was to assess the use of a blended weather dataset, consisting of CM-SAF R_s data and ERA5-Land (ERA5L) weather data, for estimating daily ET_o with FAO Penman-Monteith, in regions where ground weather data are available for just short time intervals from a sparse monitoring network. The study was conducted for irrigation seasons from year 2003 to year 2020 in Sicily (southern Italy), where neither CM-SAF radiation data nor ERA5-Land reanalysis data had hitherto been validated.

We first discuss how effective downscaling and bias correction of ET_o at regional scale could be achieved with one season of ground weather data, and we show how the spatial interpolation error of ground weather data could be statistically estimated. Then we compare the quality of CM-SAF solar radiation and ERA5L reanalysis weather data with the respective data obtained by spatially interpolating ground observations. Finally, by taking ET_o computed with ground weather data as a benchmark, we compare the accuracies of ET_o estimates at ungauged sites computed respectively with: i) spatially interpolated ground weather data; ii) only ERA5-Land weather data; iii) the ERA5-Land weather dataset blended with solar radiation retrieved from CM-SAF.

2. Study area and meteorological data

2.1. Study area

The study area was Sicily (southern Italy), the largest island in the Mediterranean with an area of about 25,000 km^2. Fig 1 shows the location and relief map of the region with its wide range of elevations from 0 m a.m.s.l. to about 3,230 m a.m.s.l. at the top of the volcano Etna in the north-eastern part of the island. The small islands surrounding the region were omitted from the study.

The weather in the study area is influenced by the topographic complexity and by the presence of the Mediterranean Sea. Under the Köppen-Geiger climate classification, the region has a hot dry-summer subtropical climate, which is also known as a "typical Mediterranean climate". Areas with this climate typically experience hot, sometimes very hot, dry summers and mild, wet winters (Peel et al., 2007). Summers in such areas can often be very similar to summers of semi-arid climates.

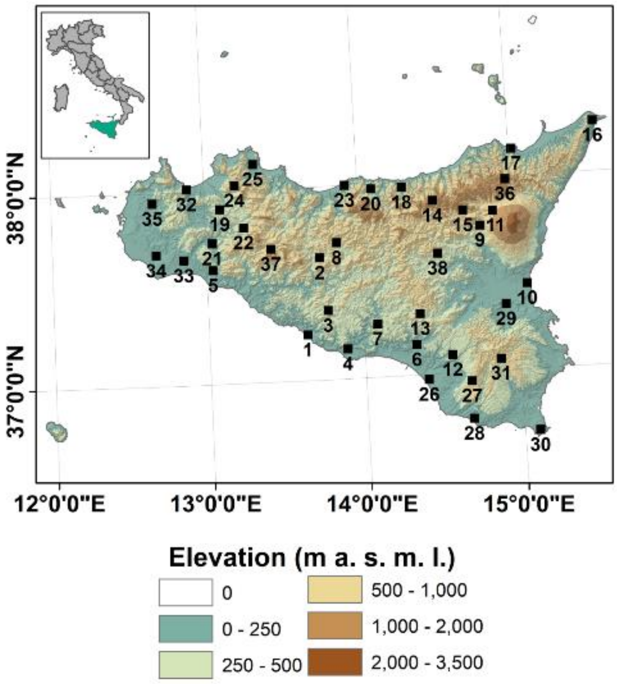

Fig.1. Relief map of the study area along with the location of the 38 automatic weather stations (AWSs) used for the analysis (Table A1)

Annual rainfall in the region varies proportionally with site elevation, from 400 mm to 1300 mm. The mean annual temperature ranges from 11 °C in mountain areas to 19 °C along the coast (Liuzzo et al., 2017). Minimum precipitation and maximum temperature occur in summer, mainly in July and August, with mean daily values close to 0 mm and 28 °C, respectively. Maximum precipitation and minimum temperature occur between December and February, with mean monthly values of 150 mm and 11 °C, respectively (Cammalleri et al., 2012).

Field irrigation generally starts in April and lasts until the end of September, although the actual time span of the irrigation season is influenced by weather fluctuations and specific cropping practices. Hereinafter, the period from April 1st to September 30th will be referred to as the irrigation season (183 days). The analyses below concern the assessment of the different weather data sources and daily reference evapotranspiration at regional scale in the irrigation seasons of the years 2003-2020.

2.2. Meteorological data

This section illustrates the different data sources employed for retrieving the input variables required to assess daily ET_o with the FAO Penman-Monteith equation: daily aggregation of air temperature, wind speed, dew point temperature/air relative humidity to estimate actual vapor pressure, incoming shortwave solar radiation, and air barometric pressure.

2.2.1. Observed ground-based data

Ground weather data were retrieved from the agrometeorological monitoring network managed by the Sicilian Agrometeorological Information Service (SIAS –*Servizio Informativo Agrometereologico Siciliano*, www.sias.regione.sicilia.it). Although the network comprises 96 automatic weather stations (AWSs), in operation since 2002, only 42 AWSs are equipped with pyranometers. Many gaps in the time series are present in year 2002 thus only data collected in the irrigation seasons of years 2003-2020 were examined in this study.

This is a post-peer-review, pre-copyedit version of an article published in *Agricultural Water Management*.
The final authenticated version is available online at: *https://doi.org/10.1016/j.agwat.2021.107169*

The quality of ground data was preliminarily verified according to Allen (1996). Pyranometer data accuracy was verified by plotting daily R_s data against computed shortwave radiation under clear sky radiation. Wind measurements were verified by comparing the cumulative wind runs of adjacent stations: we discarded those stations where the slope of the accumulation significantly differs from those of adjacent stations. Moreover, we discarded the wind speed measurements at 2 m above the ground in favor of wind speed measurements at 10 m due to the presence of local effects that invalidate the representativeness of the measures in the surroundings. We did not find anomalies in temperature and relative humidity data and, even in summer months, we did not find aridity effects in recorded data.

After the quality check, among the 42 AWSs that measure all the weather variables of interest, four stations were discarded: two (Cesarò Monte Soro and Alia) present many gaps in the time series; a third (S. Fratello) was discarded because of wind data anomalies compared with nearby stations; a fourth station was excluded because it lies on a small island north of Sicily (Salina) outside the boundaries of the study region.

Table A1 provides a list of the selected 38 AWSs along with their geographic coordinates, elevation (ranging from 10 m a.s.m.l. to 1470 m a.s.m.l.) and weather data statistics recorded in the 18 seasons of interest. Fig. 1 also shows the locations of the stations in the study region.

Table 1 summarizes some average statistics of the data recorded from April to September during the 18 years in question (2003-2020). T_{max} (°C) and T_{min} (°C) are, respectively, the daily maximum and minimum air temperature at 2 m, R_s (W m^{-2}) is the daily mean of the incoming shortwave solar radiation, u_{10} (m s^{-1}) is the daily mean of the wind speed at 10 m, e_a(kPa) is the daily mean actual vapor pressure computed from the observed daily maximum and minimum air relative humidity (RH_{max} (%) and RH_{min} (%), respectively) as follows (Allen et al., 1998):

$$e_a = \frac{e^0(T_{min})\frac{RH_{max}}{100} + e^0(T_{max})\frac{RH_{min}}{100}}{2} \qquad (1)$$

where $e^0(T_{min})$ and $e^0(T_{min})$ are the saturation vapor pressures (kPa) computed at the daily maximum and minimum air temperatures, respectively. The relation between the saturation vapor pressure (kPa) and temperature (°C) is given by the following expression (Allen et al., 1998):

$$e^0(T) = 0.6108\ exp\left[\frac{17.27\ T}{T+273.3}\right] \quad (2)$$

Table 1. Regional mean statistics of the daily weather variables of interest, based on data collected during the 18 irrigation seasons examined (2003-2020)

	Mean	Coefficient of variation
T_{max}	26.7 °C	0.13
T_{min}	15.5 °C	0.18
R_s	263 W m^{-2}	0.21
e_a	1.4 kPa	0.19
u_{10}	2.58 m s^{-1}	0.36

2.2.2. Reanalysis data

Meteorological reanalysis products provide an accurate reconstruction of the climate of the past by running back in time the most advanced and updated versions of the numerical weather prediction models that obey physical laws, while sequentially assimilating land surface and atmospheric observations from across the world. In recent years, reanalysis products have been increasingly used as a gridded data source for water resource management studies since they represent a complete and consistent climate dataset that covers several decades (Soci et al., 2016).

In this study, we employed the most advanced global reanalysis data produced in Europe, specifically optimized for the land surface applications: ERA5-Land (ERA5L), freely available at the website https://cds.climate.copernicus.eu (Muñoz Sabater, 2019). ERA5-Land is produced for the entire globe with a native horizontal resolution of about 9 km (released on a regular 0.1° x 0.1° grid) by replaying the land component of ERA5 climate reanalysis, from 1981 to 2-3 months before present. ERA5 is the fifth generation of ECMWF global reanalysis, succeeding ERA-Interim and

This is a post-peer-review, pre-copyedit version of an article published in *Agricultural Water Management*.
The final authenticated version is available online at: *https://doi.org/10.1016/j.agwat.2021.107169*

covering the entire globe from 1979 at a spatial resolution of about 31 km (Hersbach et al., 2020). The atmospheric forcing in ERA5-Land is provided by land fields of ERA5 atmospheric variables. ERA5 air temperature, air humidity and pressure are corrected to account for the elevation difference between the grid of the forcing and the higher-resolution grid of ERA5-Land, according to the so-called lapse rate correction (Muñoz Sabater, 2019).

Although ERA5-Land runs at enhanced spatial resolution, it has the drawback that data are not provided for numerical grid points falling on the sea surface. Thus, for land areas close to the coast, the assessment of weather variables must rely on the closest inland data alone. Fig. 2 shows the numerical grid of ERA5-Land only where data are available.

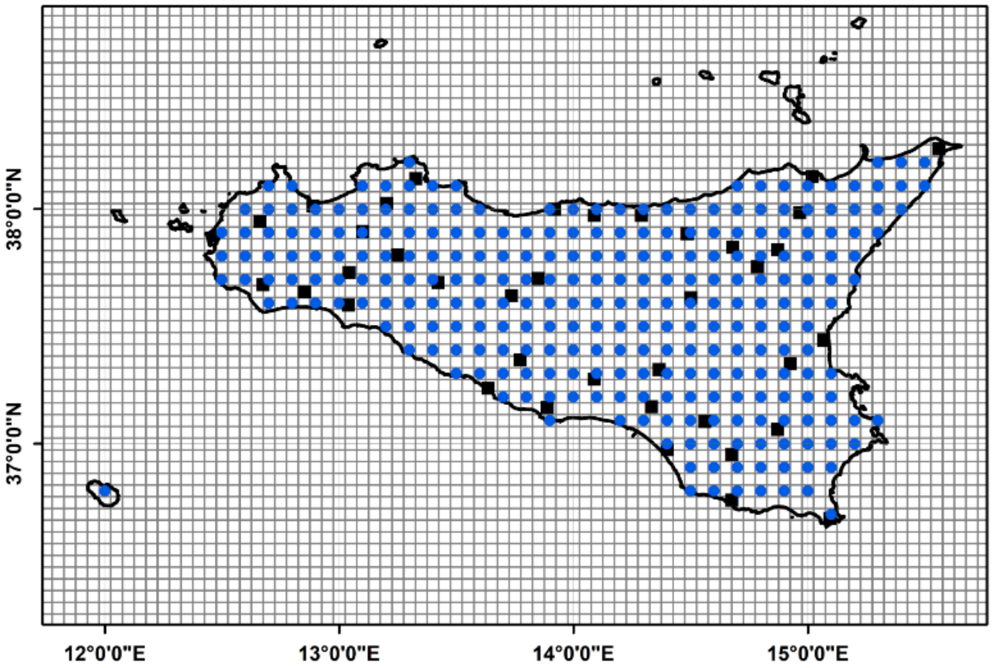

Fig. 2. Location of the (i) AWSs (black squares), (ii) ERA5-Land grid points (blue circles) and (iii) CM-SAF grid (gray mesh).

ERA5-Land data are produced with an hourly time-step. Thus, minimum, maximum, and mean daily values of the weather variables were here derived by gathering 24 values, starting from UTC+2 every day, to calculate the daily values according to the summer time as the ground weather data. The

This is a post-peer-review, pre-copyedit version of an article published in *Agricultural Water Management*.
The final authenticated version is available online at: *https://doi.org/10.1016/j.agwat.2021.107169*

selected weather variables of interest were air temperature at 2 m, wind speed at 10 m, dew point temperature at 2 m, global incoming solar radiation, and barometric pressure.

The daily mean dew point temperature was used in Eq. (2), $e_a = e^0(T_{dew})$, for computing the daily mean of the actual vapor pressure, instead of the daily maximum and minimum relative humidity, as done for the ground-based data (Eq. 1).

2.2.3. Satellite-based surface incoming shortwave solar radiation data

This subsection describes the Meteosat satellite-derived surface incoming global shortwave radiation products provided by the Satellite Application Facility on Climate Monitoring (CM-SAF). Meteosat geostationary satellites were launched by ESA (European Space Agency) and operated by the European Organization for the Exploitation of Meteorological Satellites (EUMETSAT) and the European Space Agency (ESA). Meteosat first generation (MFG) satellites were equipped with the Meteosat Visible and Infrared Imager (MVIRI). Since 2004, Meteosat Second Generation (MSG) satellites were launched. MSG satellites were equipped with the Spinning Enhanced Visible and Infrared Imager (SEVIRI) radiometers (Trigo et al., 2011; Urraca et al., 2017). MVIRI on board of MFG satellites, consists of a high-resolution 3-band radiometer, providing simultaneous image generation in the thermal infrared region (TIR), in the water vapor absorption bands (WV), and in the visible range (VIS). SEVIRI on board of MSG satellites allows the full Earth–atmosphere system to be scanned in 12 spectral channels. Both SEVIRI and MVIRI have a spatial resolution between 3 and 5 km over most of Europe (Schmetz et al., 2002).

Satellite-based climate and weather data records at the Earth's surface are made freely available for users by three independent Satellite Application Facilities (SAFs): (i) the Satellite Application Facility on Climate Monitoring (CM-SAF, www.cmsaf.eu), (ii) the Land Surface Analysis Satellite Application Facility (LSA-SAF, www.landsaf.meteo.pt) and (iii) the Ocean and Sea Ice Satellite Application Facility (OSI-SAF, www.osi-saf.org). To retrieve the satellite-based meteorological parameters, the different SAFs use their own algorithms and different ancillary input data (Journée

This is a post-peer-review, pre-copyedit version of an article published in *Agricultural Water Management*.
The final authenticated version is available online at: *https://doi.org/10.1016/j.agwat.2021.107169*

and Bertrand, 2010); currently, all of them release the data in near-real time with a lag of two days from the present.

The algorithms used for retrieving the satellite-based dataset are frequently updated and improved: in particular, the newest update regarding the CM-SAF algorithms consisted in adapting the software for processing Meteosat-11 imageries in operational mode, starting from the year 2018. Prior to 2018, CM-SAF focused on the off-line production and distribution of coherent time series of daily and monthly averaged products. LSA-SAF and OSI-SAF have been following a near real-time strategy since their establishment.

For the purpose of this study, our interest was in land surface incoming shortwave radiation products that are provided by both CM-SAF and LSA-SAF. Journée and Bertrand (2010) showed that CM-SAF outperformed LSA-SAF at both hourly and daily scales over Belgium (CM-SAF exhibited RMSE and relative RMSE 0.5% and 3.9% smaller than LSA-SAF, respectively). Thus, for the following analysis, CM-SAF radiation data were considered, although other studies successfully employed LSA-SAF products for analogous applications (e.g., Paredes et al., 2021).

The CM-SAF surface incoming short-wave radiation products are available on the Web User Interface of the CM-SAF website (http://wui.cmsaf.eu), as monthly and daily means, and as 30-min instantaneous data on a regular latitude/longitude grid with a spatial resolution of 0.05° x 0.05° degrees. The products are part of SARAH-2.1, which is a satellite-based climate data record of the solar surface irradiance, the surface direct irradiance (direct horizontal and direct normalized), the sunshine duration, spectral information, and the effective cloud albedo derived from satellite-observations of the visible channels of the MVIRI and the SEVIRI instruments onboard the geostationary Meteosat satellites.

The CM-SAF algorithm is based on the evaluation of the interaction between the atmosphere, clear sky reflection, transmission, and the top of atmosphere albedo by implementing a radiative transfer model and a look-up table method (Mueller et al., 2009; Mueller et al., 2012). Conversion

This is a post-peer-review, pre-copyedit version of an article published in *Agricultural Water Management*.
The final authenticated version is available online at: *https://doi.org/10.1016/j.agwat.2021.107169*

from the irregular satellite projection to the regular 0.05° x 0.05° geographic grid is then performed with a gridding tool based on a nearest-neighbor method.

The CM-SAF daily estimates of surface solar radiation were successfully validated against ground-based measurements, belonging to the Baseline Surface Radiation Network (BSRN – Ohmura et al., 1998). The results of validation showed mean absolute errors on average equal to 11.8 W m^{-2} (close to the optimal accuracy of 12 W m^{-2} and much lower than the target value of 20 W m^{-2}); moreover, about 83 % of values met the optimal accuracy requirement while 100% of values were found to be lower than the target value. The CM SAF User Manual and Validation Report document the implemented algorithms and the accuracy of SARAH-2.1 climate data record with reference to the BSRN (Pfeifroth et al., 2018).

In this study, daily means of surface incoming short-wave radiation data for the irrigation seasons of years 2003-2020 were employed. Fig. 2 shows the CM-SAF grid (gray mesh) over the study area.

3. Methods

3.1. Downscaling and bias correction of reanalysis and satellite-based data at the AWS sites

The procedure that is used to transfer the weather information from the points of a regular grid to other sites within this grid is a form of downscaling, which is more often referred to as the method for inferring information from a low-resolution to high-resolution grid. Here, statistical downscaling techniques were used to infer reanalysis and satellite-based data from the native grid of the databases of interest to the AWS sites. Downscaled data were then bias-corrected to remove the residual systematic errors from the estimates.

This is a post-peer-review, pre-copyedit version of an article published in *Agricultural Water Management*.
The final authenticated version is available online at: *https://doi.org/10.1016/j.agwat.2021.107169*

3.1.1. Downscaling of reanalysis weather data

To retrieve the reanalysis weather data at the AWS sites from the 0.1° x 0.1° numerical grid, a triangle-based bi-linear interpolation method was employed (Lee and Schachter, 1980). The method consists in interpolating the three grid points closest to the examined site.

Since evident statistical correlations were found between the daily maximum and minimum temperatures and terrain elevation, before proceeding with the grid interpolation of these two weather variables, a so-called environmental lapse rate (ELR) correction was applied to the grid points of interest for interpolation, in order to consider the elevation differences between the grid points and each AWS site. The ELR correction was then applied to three nearest grid points to be used for interpolation to each AWS site as follows:

$$T_{ELR} = T_{GD} + (z - z_{GD})\, ELR \qquad (3)$$

where z stands for the elevation of the AWS site, z_{GD} refers to the elevation of the numerical grid point of interest for interpolation, T_{GD} is the raw reanalysis temperature value at this numerical grid point, and T_{ELR} is the ELR corrected temperature value at the grid point of interest for interpolation at the chosen AWS site.

The environmental lapse rate is defined as the rate of temperature change with elevation:

$$ELR = \frac{dT}{dz} \qquad (4)$$

It can be computed from observations of temperature at *m* sample sites by implementing a linear regression model with the elevation, z:

$$\hat{T} = ELR\, z + T_0 \qquad (5)$$

where ELR is the slope of the regression line and T_0 is the intercept, both computed with the ordinary least squares (OLS) method.

Since the ELR depends on complex factors such as overlying air masses, the large-scale situation, and local effects (Sheridan et al., 2010), its estimation represents a challenging task. However, the use of a linear lapse rate for elevation correction between model and station temperature

This is a post-peer-review, pre-copyedit version of an article published in *Agricultural Water Management*.
The final authenticated version is available online at: *https://doi.org/10.1016/j.agwat.2021.107169*

is common practice in hydrological and environmental applications (e.g., Gupta and Tarboton, 2016). Moreover, the use of a linear ELR computed from ground-based observations, when available, is generally accepted and preferred to the use of the common reference value of –0.0065 °C m^{-1} (Rolland, 2003; Gao et al., 2015), especially for complex terrain. This approach has two main limitations: (i) it relies on the elevation variability among the stations, and (ii) it assumes that temperature recorded by stations at different elevations is representative of the mean lower troposphere vertical profile, even if the near-surface temperature gradient may be dominated by the surface energy balance, surface roughness, and near-surface boundary layer effects, rather than by adiabatic effects and the current stratification of the atmosphere (Gao et al., 2015; Dutra et al., 2020). Thus, downscaled reanalysis temperature data are still affected by systematic errors due to the dependence of daily temperatures on local terrain attributes other than elevation.

In this study, the described ELR correction approach was applied to daily maximum and minimum temperatures by using not only the 38 complete AWSs selected for the study but all the 96 AWSs equipped with the temperature sensor. The elevations of these AWSs range from 10 m a.s.m.l. to 1875 m a.s.m.l.: a complete list of them can be found on the SIAS website (www.sias.regione.sicilia.it). Moreover, ELR correction was done here on a monthly basis by performing six linear regression analyses to obtain six ELR values for each month, from April to September.

3.1.2. Downscaling of satellite-based radiation data

To retrieve the satellite-based surface shortwave radiation data at the AWS sites from the 0.05° x 0.05° CM-SAF grid, the nearest grid point was considered since the satellite product is a pixel-integrated measurement of the parameter of interest. An important aspect to consider for understanding the differences between ground measurements at sites and satellite-derived information, is the fact that satellite data are a snapshot over a large area (i.e., the pixel) which does

This is a post-peer-review, pre-copyedit version of an article published in *Agricultural Water Management*.
The final authenticated version is available online at: *https://doi.org/10.1016/j.agwat.2021.107169*

not account for the variability of the parameter within the pixel size, while ground information is a time-integrated local measurement (Journée and Bertrand, 2010).

3.1.3. Bias correction of downscaled reanalysis and satellite-based weather variables

Estimates from numerical weather prediction models and satellite-based products suffer from systematic and non-systematic errors, which originate from various sources, such as sub grid-scale variability and inability of the models to fully describe the physical phenomena (Journée and Bertrand, 2010; Pelosi et al., 2017). Statistical postprocessing techniques can partly remove such errors. Among such techniques, batch statistical methods are calibrated offline with a training dataset that can be of a short length if a parsimonious number of parameters are required (Vannitsem, 2008). Moreover, simple bias correction approaches are often preferred to more sophisticated post-processing techniques, since no significant loss in accuracy is noted despite the much lower computation costs (e.g., Paredes et al., 2018).

In this study, a regionally uniform bias correction at monthly scale was applied to all variables except for wind speed, for which no systematic bias pattern was found, consistent with previous reports (Ricard and Anctil, 2019; Pelosi et al., 2020a). The applied method consists in adding to the downscaled products the monthly regional mean difference (bias) between the ground-based measurements and the respective downscaled data, computed over the calibration period.

The first six years (2003-2008) were chosen as calibration period while the remaining 12 years (2009-2020) were used for creating the validation set to which the performance statistics refer. The bias correction was applied in the scenario where ground weather observations were not available for the period of interest, but data from few past irrigation seasons (e.g., here six seasons) were available for calibration.

3.2. Assessing spatial interpolation error of ground-based data by cross-validation at the AWS sites

Ground-based measurements are often available over irregularly spaced and sparse monitoring networks. Thus, spatial interpolation techniques must be employed if data are required at specific

This is a post-peer-review, pre-copyedit version of an article published in *Agricultural Water Management*.
The final authenticated version is available online at: *https://doi.org/10.1016/j.agwat.2021.107169*

ungauged locations or according to a regular grid, such as those of numerical products. Among the extensive range of spatial interpolation methods, geostatistical techniques are the most advanced and used for weather applications (Hofstra et al., 2008).

Ordinary kriging is the most widely used technique to interpolate weather data, such as wind speed (Luo et al., 2008; Berndt and Haberlandt, 2018; Pelosi et al., 2020a), relative humidity (Berndt and Haberlandt, 2018; Pelosi et al., 2020a) and solar radiation (Rehman and Ghori, 2000; Alsamamra et al., 2009; Journée and Bertrand, 2010; Pelosi et al., 2020a). However, ordinary kriging only uses data available from observations and its performance significantly depends on the density of the available monitoring network and the spatial properties of the variable of interest (Prudhomme and Reed, 1999; Pelosi and Furcolo, 2015). For this reason, in some other applications where an evident statistical correlation exists between the weather variable of interest and an auxiliary external variable sampled with a higher spatial resolution, regression kriging is preferred (Jarvis and Stuart, 2001; Pelosi et al., 2020a). This is the case of temperature (Jarvis and Stuart, 2001; Stahl et al., 2006; Di Piazza et al., 2015; Pelosi et al., 2020a), which shows a high correlation with elevation.

Regression kriging (Odeh et al., 1995), also known as residual kriging (Holdaway, 1996) and mathematically equivalent to universal kriging, often referred to as kriging with external drift (Ahmed and de Marsily, 1987), applies ordinary kriging to the regression residuals of a regression model between the variable of interest and auxiliary independent variables.

In this study, ordinary kriging was used for interpolating daily wind speed, maximum and minimum relative humidity, and solar radiation. Regression kriging was employed for daily maximum and minimum air temperature, by implementing daily linear regression models of temperature with elevation. Appendix B summarizes the theoretical bases of the geostatistical methods applied herein; more details can be found in Journel and Huijbregts (1978) and Cressie (1993).

This is a post-peer-review, pre-copyedit version of an article published in *Agricultural Water Management*.
The final authenticated version is available online at: *https://doi.org/10.1016/j.agwat.2021.107169*

Since the focus of this study was on evaluating the performance of the spatial interpolation of ground-based data, a leave-one-out cross-validation technique was recursively implemented to compute the jackknife kriging estimation of the variable of interest at each AWS site, after applying the kriging interpolator to the observations available at the remaining sampling sites. This is a very common way to assess the predictive ability of a statistical model and, specifically, of a geostatistical interpolation technique. The result was a set of interpolated ground-based data (IGD) at each AWS site that could be compared with the measurements recorded at the same site, for evaluating the performance of the kriging interpolator.

3.3. Computation of reference daily evapotranspiration (ET$_o$)

In this study, the daily reference evapotranspiration, ET$_o$ (mm day^{-1}) was computed with the FAO Penman–Monteith equation (Allen et al., 1998), as follows:

$$\mathrm{ET_o} = \frac{1}{\lambda}\frac{\Delta\,(\mathrm{R_n} - \mathrm{G}) + \gamma\frac{900}{\mathrm{T}+273}\,\mathrm{u_2}\,(e_s - e_a)}{\Delta + \gamma_p(1 + 0.34\mathrm{u_2})} \qquad (6)$$

where λ is the latent heat of vaporization, equal to 2.45 MJ kg^{-1}; Δ (kPa °C^{-1}) is the slope of the vapor pressure curve; γ is the psychometric constant (kPa °C^{-1}); T (°C) is the daily mean air temperature at 2 m height computed as the average between the daily maximum (T$_{max}$) and minimum (T$_{min}$) air temperature at 2 m height; u$_2$ (m s^{-1}) is the wind speed at 2 m height above ground; e$_s$ (kPa) and e$_a$(kPa) are, respectively, the daily saturation vapor pressure and daily actual vapor pressure (Equations 1-2) needed for the computation of the saturation vapor pressure deficit (e$_s$ -e$_a$); R$_n$(MJ m^{-2} day^{-1}) is the net radiation at the crop surface and G (MJ m^{-2} day^{-1}) is the soil heat flux density. The net radiation (R$_n$) was calculated as the difference between the incoming net shortwave radiation and the outgoing net long-wave radiation. The incoming net shortwave radiation is a fraction of the incoming shortwave solar radiation (R$_s$), computed for the reference crop by setting the albedo equal to 0.23.

This is a post-peer-review, pre-copyedit version of an article published in *Agricultural Water Management*.
The final authenticated version is available online at: *https://doi.org/10.1016/j.agwat.2021.107169*

The daily mean wind speed at 2 m, u_2 (m s^{-1}), was obtained from the wind speed at 10 m, u_{10} (m s^{-1}), by using a logarithmic wind speed profile as suggested by Allen et al. (1998):

$$u_2 = u_z \frac{4.87}{\ln{(67.10\, z - 5.42)}} \tag{7}$$

where z = 10 m, resulting in a reduction factor to apply to u_z of about 0.748 for obtaining the wind speed at the lower height of 2 m.

More details about the parameters in Eq. (6) can be found in the FAO irrigation and drainage study No. 56 (Allen et al., 1998) and are omitted herein for the sake of brevity.

Table 2. Monthly statistics of the daily reference evapotranspiration over the region, based on data recorded during 18 irrigation seasons (2003-2020)

ET_o (mm day^{-1})	Mean	Coefficient of variation
April	3.26	0.31
May	4.28	0.26
June	5.24	0.21
July	5.75	0.14
August	5.10	0.18
September	3.56	0.25

Table 2 reports monthly statistics of daily ET_o averaged between the 38 AWSs over the irrigation seasons of the years 2003–2020. The minimum monthly mean of daily ET_o was recorded in April (3.26 mm day^{-1}) and the maximum in July (5.75 mm day^{-1}). The mean coefficient of variation was lowest in July (0.14) and highest in April (0.31).

3.4. Scenarios of ET_o estimates

The daily reference evapotranspiration, ET_o, computed at the AWS sites with ground-based data was taken as the benchmark for comparing the performance of ET_o estimated with three alternative weather data sets:

- IGD, weather data obtained by spatial interpolation with the leave-one-out cross-validation technique;

- ERA5L, weather data retrieved after downscaling and bias-correcting ERA5-Land reanalysis data;
- ERA5L+CM-SAF, obtained by changing ERA5L shortwave incoming solar radiation with downscaled and bias-corrected CM-SAF solar radiation data.

Table 3. Scenarios of ET_o estimates examined in this study

Data availability scenario	**Scenario name**	**Dataset composition method**	**Data source**		
			AWS	ERA5-Land	CM-SAF
Ground weather data available at AWS sites	IGD	Spatial interpolation is used for all weather data	x	-	-
Ground-based weather data are not available $^{(*)}$	ERA5L	All weather data are retrieved from reanalysis products	-	x	-
	ERA5L + CM-SAF	R_s by satellite-based products, remaining data from reanalysis	-	x	x

$^{(*)}$ Bias correction was performed by using only six of the available past seasons data (calibration period) out of the period of interest (the remaining 12 seasons consist in the validation set)

The three scenarios of ET_o estimates examined in this study are summarized in Table 3. IGD refers to the scenario when ground weather data are available for the entire period of interest and thus interpolation is the only error source at regional scale. ERA5L and ERA5L+CM-SAF scenarios refer to the case when data from the ground monitoring network are available for only a limited period (e.g., one season) to be used for regional bias correction, and thus ERA5L and CM-SAF are used as alternative data sources.

3.5. Indicators of estimation performance

The performance indicators were selected among those commonly used for analogous previous studies (e.g., Paredes et al., 2018; Paredes et al., 2021):

(i) The percent BIAS (PBIAS, %), which is used as an indicator of accuracy:

$$\text{PBIAS (\%)} = \frac{1}{\bar{O}} \frac{\sum_{i=1}^{n}(P_i - O_i)}{n}\, 100 \qquad (8)$$

where P_i and O_i are, respectively, the variable for which the performance evaluation is desired and the corresponding observed variable (benchmark) at the ith day; n denotes the number of examined days and $\bar{O}$ is the mean of the observations computed over the examined days. The more the PBIAS differs from zero, the less accurate is the estimate. PBIAS <0 suggests on average underestimation while PBIAS >0 overestimation.

(ii) The normalized root mean square error (NRMSE, %) which gives insight into both accuracy and precision:

$$\text{NRMSE (\%)} = \frac{1}{\bar{O}}\sqrt{\frac{\sum_{\text{i}=1}^{n}(P_i - O_i)^2}{n}}\ 100 \qquad (9)$$

The greater is the NRMSE, the less accurate and precise are the estimates.

(iii) The coefficient of determination (R^2) of the OLS regression model used to assess the dispersion of pairs of O_i and P_i (independent variable) values along the regression line:

$$\text{R}^2 = \frac{\sum_{\text{i}=1}^{n}(\hat{O}_i - \bar{O})^2}{\sum_{\text{i}=1}^{n}(O_i - \bar{O})^2} \qquad (10)$$

where $\hat{O}_i$ is the predicted value by the linear regression $\hat{O}_i = a + b\ P_i$. R^2 may vary from 0 to 1: the closer R^2 values are to 1, the larger the fraction of the variance of the observations explained by the model.

(iv) The Nash and Sutcliffe (1970) model efficiency (NSE) is equal to one minus the sum of the absolute squared differences between the predicted and observed values normalized by the variance of the observed values during the period of interest (Krause et al., 2005):

$$\text{NSE} = 1 - \frac{\sum_{\text{i}=1}^{n}(P_i - O_i)^2}{\sum_{\text{i}=1}^{n}(O_i - \bar{O})^2} \qquad (11)$$

The range of NSE lies between 1 (perfect model with an estimation error variance equal to zero) and $-\infty$. Values of NSE nearer to 1 suggest a model with more predictive skill. NSE equal to 0 indicates that the model has the same predictive skill as the mean of the data, in terms of the sum of the squared error. An NSE value lower than zero indicates that the mean value of the observed data would have been a better predictor than the model that

This is a post-peer-review, pre-copyedit version of an article published in *Agricultural Water Management*.
The final authenticated version is available online at: *https://doi.org/10.1016/j.agwat.2021.107169*

shows an estimation error variance which is significantly larger than the variance of the observations.

Bias-corrected reanalysis and satellite-based data were employed in the hypothesis that users have only few irrigation seasons available for bias correction, so the calibration period was created by one third of the available seasons.

4. Results and discussion

4.1. Performance of weather variable products

The following results refer to the performance of the spatially interpolated ground-based daily weather data (IGD) and the downscaled bias-corrected ERA5L reanalysis and satellite-based (CM-SAF) daily products at the 38 AWSs of the region in the irrigation seasons of the years 2018-2020. Appendix C presents the performance of reanalysis (ERA5L) and satellite-based (CM-SAF) daily weather variables before and after the regional mean bias correction, also discussed in this section.

The variability of the performance indicators computed at the 38 AWS sites is illustrated with boxplots: on each box, the central mark is the median, the edges of the box are the 25th (q_1) and 75th (q_3) percentiles, the whiskers extend to the most extreme data values not considered outliers, and outliers are plotted individually. The points are drawn as outliers if they are larger than $q_3 + 1.5(q_3 - q_1)$ or smaller than $q_1 - 1.5(q_3 - q_1)$. The circle mark represents the mean value among the AWS sites.

4.1.1. Air temperature

ERA5L reanalysis daily maximum and minimum temperature data were downscaled by monthly ELR corrections (as described in Section 3.1.1) whose estimates were obtained by OLS regression of ground-based observations with elevation. Table 4 reports the monthly ELR coefficients for T_{max} and T_{min} along with coefficient of determination, R^2_{ELR}.

Table 4. Monthly environmental lapse rates (ELR) estimated for downscaling the daily T_{max} and T_{min}

	APR	MAY	JUN	JUL	AUG	SEP

This is a post-peer-review, pre-copyedit version of an article published in *Agricultural Water Management*.
The final authenticated version is available online at: *https://doi.org/10.1016/j.agwat.2021.107169*

T_{max}	**ELR**	-0.0064	-0.0060	-0.0051	-0.0047	-0.0046	-0.0060
	R^2_{ELR}	0.82	0.64	0.43	0.36	0.40	0.73
T_{min}	**ELR**	-0.0035	-0.0033	-0.0027	-0.0029	-0.0033	-0.0045
	R^2_{ELR}	0.46	0.41	0.30	0.32	0.39	0.62

Absolute ELR values are lower for the daily minimum temperature than for the daily maximum temperature, in accordance with a similar study that applied lapse rate corrections to ERA5 reanalysis temperature data in Western US (Dutra et al., 2020). These results were expected, since low-level conditions during the night tend to be more stable, resulting in less intense ELR for the daily T_{min}. Moreover, consistent with the current study, Dutra et al. (2020) highlighted that ERA5 T_{min} bias is less dependent on elevation than T_{max}, resulting in a lower coefficient of determination (Table 4). The same reason explains the lower performance of ERA5L T_{min} before and after bias correction than raw ERA5L T_{max} (Figs. C1 and C2). The mean regional PBIAS values of ERA5L daily T_{max} and T_{min} products before bias correction are about -4% and 7%, respectively (Figs. C1 and C2), indicating a tendency to underestimate T_{max} and overestimate T_{min}. Similar findings were reported in the cited study by Dutra et al. (2020) as regards ERA5 products in Western US and in many other studies that evaluated the ERA-Interim reanalysis database in different regions of the world (among others, see Fu et al., 2016; Martins et al., 2017; Paredes et al., 2018). The NCEP/NCAR reanalysis products also showed T_{max} estimates outperforming T_{min} estimates as well as the tendency to overestimate T_{min} (Srivastava et al., 2015). Despite the great progress in atmospheric modeling and resolution, representation of near-surface daily maximum and especially minimum temperature in reanalysis products suffers from these systematic biases, due to large model limitations in representing clouds, radiation, boundary layer, and land surface characteristics (Dutra et al., 2020). However, the random component of the errors was greatly improved in ERA5 with respect to the former ERA-Interim, due to a better synoptic scale variability and resolution, as is also evident from a recent study that compared ERA5-Land reanalysis with UERRA, which is a regional reanalysis forced by ERA-Interim (Pelosi et al., 2020a).

This is a post-peer-review, pre-copyedit version of an article published in *Agricultural Water Management*.
The final authenticated version is available online at: *https://doi.org/10.1016/j.agwat.2021.107169*

The systematic errors were successfully removed by means of the bias correction technique explained in Section 3.1.4: Figs. C1 and C2 show that the mean PBIAS was reduced to almost zero for T_{max} and to lower than 3% for T_{min}. The NRMSE, R^2 and NSE were also slightly improved.

IGD shows a slight tendency to overestimate the observed T_{max} while ERA5L, after bias correction, has a non-systematic tendency to overestimate or underestimate T_{max}. As shown by Fig. 3a, on average both the PBIAS values of IGD and ERA5L products are quite low, varying from 14.5 % for IGD to 0.61 for ERA5L, indicating excellent accuracy. Then, in terms of NRMSE, R^2 and NSE, IGD just slightly outperforms on average ERA5L. The NRMSE values reach 17% for IGD and 10% for ERA5L, with mean values of 5.9% and 6.3%, respectively. R^2 is on average equal to 0.96 and 0.94 for IGD and ERA5L, respectively. Moreover, R^2 is always greater than 0.85. NSE is on average equal to 0.90 and 0.89 for IGD and ERA5L, respectively: it is always positive and greater than 0.43, indicating that both products have good predictive skills all over the region.

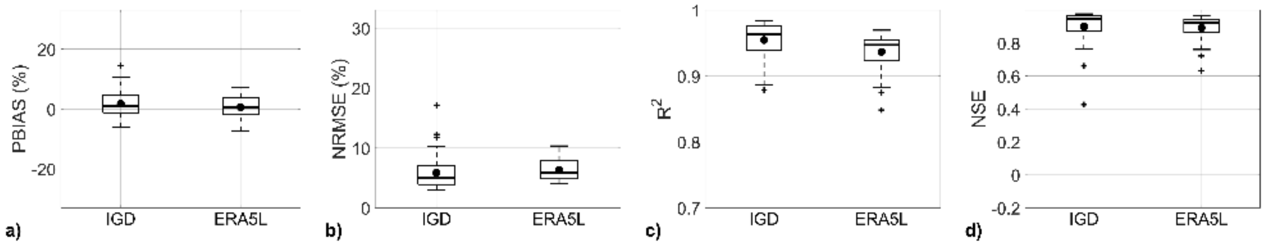

Fig. 3. Statistical indices of daily T_{max} at 38 AWS sites (validation set)

With regard to the daily minimum temperature T_{min}, both IGD and ERA5L show slightly worse performances than the results obtained for T_{max}. The main reason for this outcome lies in the dependence of T_{min} on local topographic conditions besides elevation, such that neither a spatial interpolation method (like regression kriging with elevation) nor an ELR correction with elevation are able to reproduce its variability.

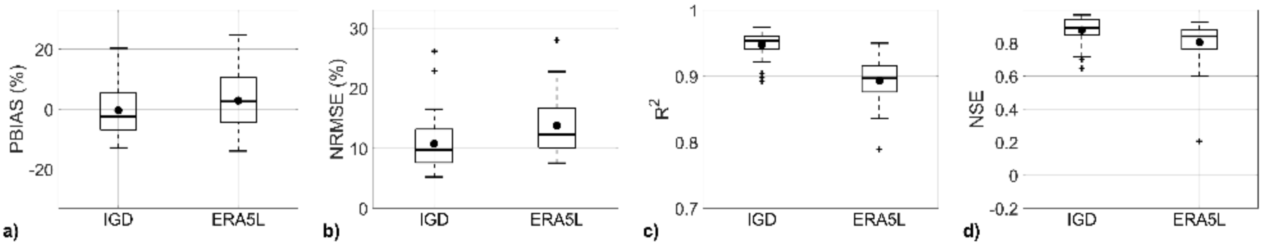

Fig. 4. Statistical indices of daily T_{min} at 38 AWS sites (validation set)

Fig. 4a shows that, on average, both the PBIAS values of IGD and ERA5L products are very low, varying from -0.35% for IGD to 2.9 for ERA5L. In terms of NRMSE, R^2 and NSE, IGD just slightly outperforms ERA5L. The maximum NRMSE is equal to 26% for IGD and 28% for ERA5L with mean values of 11% and 14%, respectively. R^2 is on average equal to 0.95 and 0.89 for IGD and ERA5L, respectively. Moreover, R^2 is always greater than 0.79. NSE is on average 0.88 and 0.81 for IGD and ERA5L, respectively: it is always positive and greater than 0.21, indicating that both products have quite good predictive skills all over the region.

4.1.2. *Wind speed*

Both IGD and ERA5L products show estimation performance for daily mean wind speed at 10 m (u_{10}) with large variability in the region of interest. ERA5L refers to the raw data, since bias correction does not improve performance (Fig. C3), consistent with previous reports (Ricard and Anctil, 2019; Pelosi et al., 2020a). As shown by Fig. 5a, PBIAS values range from -56% to 76% with a mean value of -17% for IGD, and from -62% to 38% with a mean of -21% for ERA5L. NRMSE values reach 86% for IGD and 72% for ERA5L, with mean values of 33% and 40%, respectively (Fig. 5b), indicating poor accuracy and precision of the estimates. R^2 is on average equal to 0.59 and 0.44 for IGD and ERA5L, respectively, while NSE is on average negative for both data, indicating estimation error variances that are significantly larger than the observation variance (Fig. 5c-d).

u_{10} is underestimated in more than half of the AWS sites with a poor quality of estimation for both datasets mainly due to the fact that representativeness of the wind measurements at some monitoring stations can be influenced by local terrain effects. However, the ground records are the

This is a post-peer-review, pre-copyedit version of an article published in *Agricultural Water Management*.
The final authenticated version is available online at: *https://doi.org/10.1016/j.agwat.2021.107169*

only available benchmark data: in this study to reduce the influence of local effects, measurements of wind speed at 10 m above the ground were preferred to measurements of wind speed at 2 m. Then, the daily mean wind speed at 2 m, u_2, was obtained from the wind speed at 10 m, u_{10}, by using a logarithmic wind speed profile as suggested by Allen et al. (1998) and recalled in Eq. (7).

The low accuracy and precision of reanalysis wind speed values were also reported in other studies, among which it is worth recalling the extensive study that evaluated the performance of the former ERA-Interim reanalysis database in Portugal undertaken by Paredes et al. (2018) and the study by Pelosi et al. (2020a) that analyzed ERA5-Land performance in another Italian region. To our knowledge, studies evaluating ERA5 wind speed performance for hydrological and agricultural applications at regional scale are not yet available.

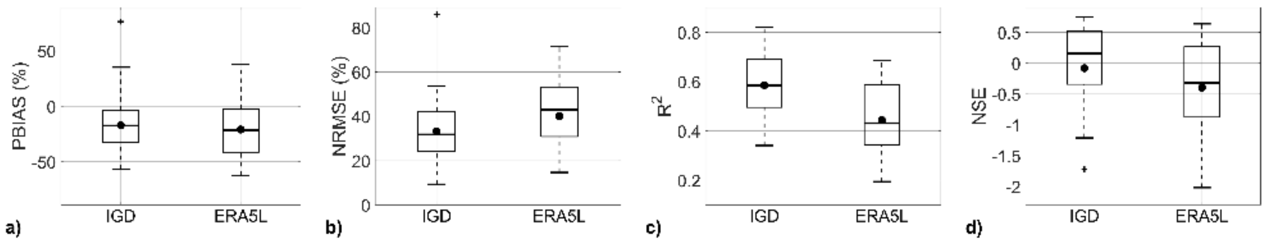

Fig. 5. Statistical indices of daily u_{10} at 38 AWS sites (validation set)

4.1.3. *Actual vapor pressure*

The daily actual vapor pressure (e_a) was derived herein for IGD from maximum and minimum relative humidity and temperature (Eq. 1) and for ERA5L from the dew point temperature (Eq. 2, with $T = T_{dew}$), according to the type of variables available for each dataset. The performance indicators for e_a show moderate spatial variability in the region, both for the case of interpolated ground-based data and for reanalysis products. As shown by Fig. 6a, PBIAS values range from -18% to 17% with a mean value of 1.7% for IGD, and from -20% to 13% with a mean of 0.12% for ERA5L, with IGD showing a slight overestimation. Raw ERA5L e_a values show systematic overestimation (mean PBIAS equal to 15% as shown in Fig. C4) which can be efficiently removed by bias correction. The NRMSE values reach 21% for IGD and 23% for ERA5L, with mean values of 14% for both

This is a post-peer-review, pre-copyedit version of an article published in *Agricultural Water Management*.
The final authenticated version is available online at: *https://doi.org/10.1016/j.agwat.2021.107169*

databases (Fig. 6b). R^2 is on average equal to 0.74 while NSE is on average 0.64 for both IGD and ERA5L (Fig. 6c-d).

In summary, IGD and ERA5L show comparable moderate accuracies in e_a estimates, consistent with the results of a previous study regarding the use of ERA5L in another region of southern Italy (Pelosi et al., 2020a).

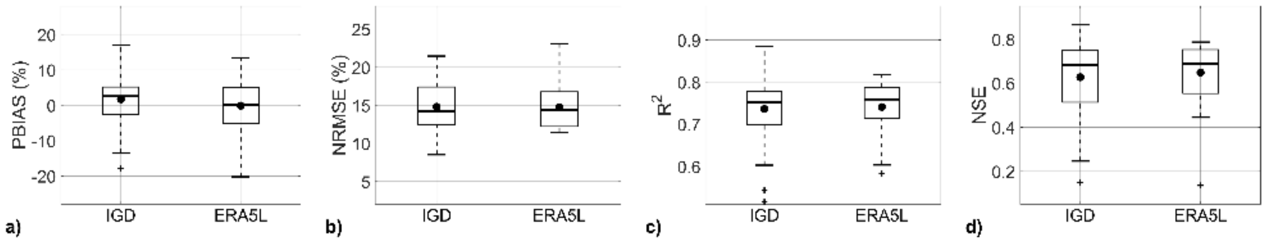

Fig. 6. Statistical indices of daily e_a at 38 AWS sites (validation set)

4.1.4. Incoming shortwave solar radiation

The ERA5L and CM-SAF incoming shortwave solar radiation (R_s) data show a mean regional PBIAS of about 3.7% and 4.7% before bias correction, respectively (Fig. C5), indicating slight overestimation. The NRMSE of CM-SAF R_s is about 5% smaller than ERA5L. The chosen bias correction technique completely removes the systematic errors with slight benefits on the other indices that remain almost unchanged (Fig. C5).

Below we illustrate the performance of the bias-corrected ERA5L and CM-SAF R_s values downscaled at the AWS sites. PBIAS values range: (i) from -6% to 12% with a mean value of 0.10% for IGD; (ii) from -8% to 10% with a mean of 1.7% for ERA5L, and (iii) from -7% to 4% with a mean of -2.4% for CM-SAF (Fig. 7a). NRMSE values reach 21% for IGD, 24% for ERA5L and 18% for CM-SAF with mean values of 10%, 14% and 9%, respectively (Fig. 7b). Moreover, NRMSE is lower than 10% for 68% and 76% of the AWS sites, respectively for the IGD and CM-SAF estimates. R^2 values are on average equal to 0.86 for IGD, 0.73 for ERA5L and 0.90 for CM-SAF, for which the minimum R^2 value is 0.75. Average NSE values are equal to 0.85 for IGD, 0.70 for ERA5L and 0.88 for CM-SAF, for which the minimum NSE value is 0.73 (Fig. 7c-d).

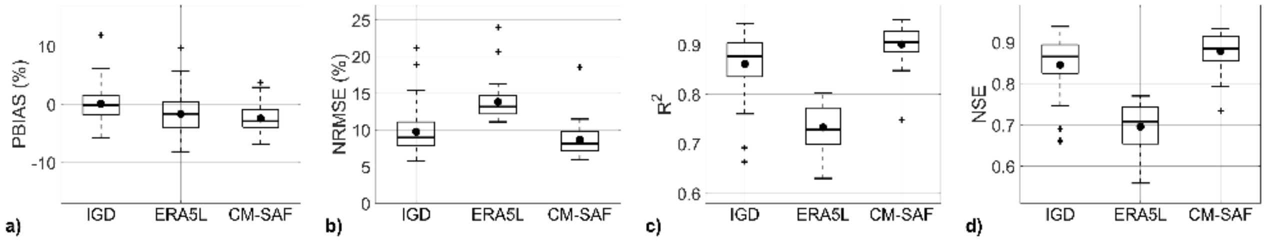

Fig. 7. Statistical indices of daily R_s at 38 AWS sites (validation set)

With regard to IGD R_s, similar results were obtained in a region of southern Italy with an analogous monitoring network density, showing an average NRMSE of ground-based solar radiation data equal to 15% (Pelosi et al., 2020a).

In the study area CM-SAF R_s clearly outperforms IGD R_s, suggesting that it is worth using satellite-based data, even when ground observations are available in the study area, for the regional assessment of environmental variables that depend on R_s. A similar suggestion was made by Paredes et al. (2021) who advised the use of LSA-SAF radiation products coupled with ground-based observations of other weather variables for assessing ET_o in near-real time. The performance of CM-SAF R_s achieved in Sicily was very close to that verified by Paredes et al. (2021) with LSA-SAF R_s in continental Portugal.

Paredes et al. (2021) also found that LSA-SAF R_s largely outperforms ERA5 R_s, for which they found a mean NRMSE of 22%, thus also larger than what we verified for ERA5-Land in Sicily. This result was expected, since ERA5-Land reanalysis benefits from higher spatial resolution (9 km vs 31 km) and specific land corrections implemented for downscaling ERA5-Land from ERA5. A similar comparative study regarding R_s products from different sources was performed by Urraca et al. (2017), who compared CM-SAF R_s and ERA-Interim R_s with ground-based data collected at a broad network of about 300 monitoring stations distributed all over Europe. Their results showed NRMSE of about 18% for CM-SAF, in perfect accordance with our findings, and about 33% for ERA-Interim. ERA-Interim reanalysis products are outperformed by both ERA5 and ERA5-Land as expected, thanks to advances in atmospheric modeling.

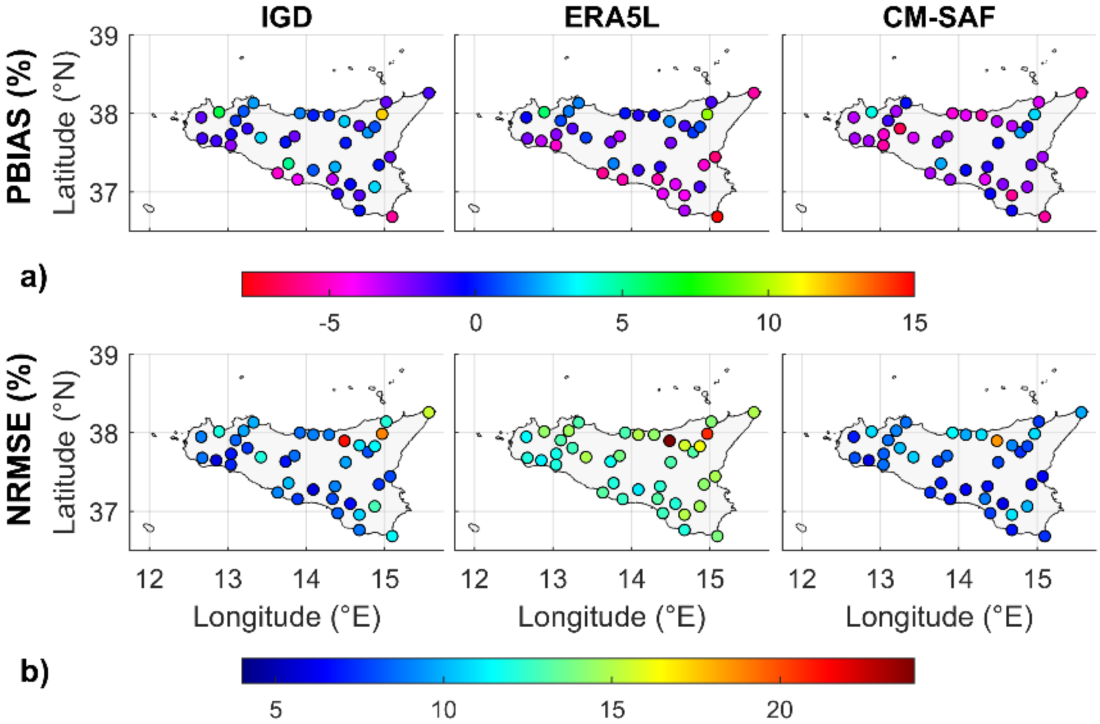

Fig. 8. Spatial depiction of the statistical indices PBIAS and NRMSE computed at the AWS sites, averaged over the validation set and related to the three different daily radiation datasets: (i) spatial interpolated ground-based data (IGD), (ii) bias-corrected ERA5-Land data and (iii) bias-corrected CM-SAF data

Fig. 8 shows the regional spatial variability of mean PBIAS and NRMSE computed over the validation set at the AWS sites. The color scales were tuned such that blue corresponds to better performances for both indices: values close to zero for the case of PBIAS and low values for NRMSE. All datasets show similar spatial patterns of performance indicators, although ERA5L is clearly outperformed by both IGD and CM-SAF, especially for NRMSE (Fig. 8b).

The area with the worst performance is north-eastern Sicily, where the most complex and highest mountain chain of the region is located. These findings are in agreement with the results of other studies reporting lower accuracy of reanalysis and satellite-based products for hill and mountain locations (Journée and Bertrand, 2010; Cristóbal and Anderson, 2013; Paredes et al., 2021). This outcome can be explained by the large sub grid-scale variability and heterogeneity of the terrain and weather conditions of hill and mountain areas that result in the inability of pixel-integrated data, such as satellite data, and coarse numerical model grids of reanalysis data to be representative of the pinpoint measurements. With regard to IGD, the reason for the worst performances observed in mountain areas should be found in the local non-stationarities of the random field as often observed in orographic areas for other variables, such as rainfall (Furcolo et al., 2016).

4.2. Performance of reference evapotranspiration estimates

This subsection reports the performance assessment of the daily FAO Penman-Monteith ET_o computed according to the three scenarios summarized in Table 3. The acronym IGD is used for ET_o estimates derived by interpolating ground-based weather variables, ERA5L stands for ET_o estimates derived by using downscaled bias-corrected ERA5L products and, finally, ERA5L+CM-SAF refers to ET_o estimates derived by using downscaled bias-corrected ERA5L products except for the incoming shortwave radiation that was substituted with bias-corrected satellite CM-SAF data.

As shown in Fig. 9a, PBIAS values range: (i) from -12% to 22% with a mean value of 5.5% for IGD; (ii) from -17% to 19% with a mean of 2.3% for ERA5L; and (iii) from -20% to 18% with a mean of 2.8% for ERA5L+CM-SAF, indicating good accuracy for all three methods. The NRMSE values reach maximum values of 27% for IGD, 22% for ERA5L and 20% for ERA5L+CM-SAF and mean values of 13%, 14% and 12%, respectively (Fig. 9b). R^2 values are on average equal to 0.85 for IGD, 0.76 for ERA5L and 0.83 for ERA5L+CM-SAF, while average NSE values are equal to 0.66 for IGD, 0.67 for ERA5L and 0.73 for ERA5L+CM-SAF (Fig. 9c-d).

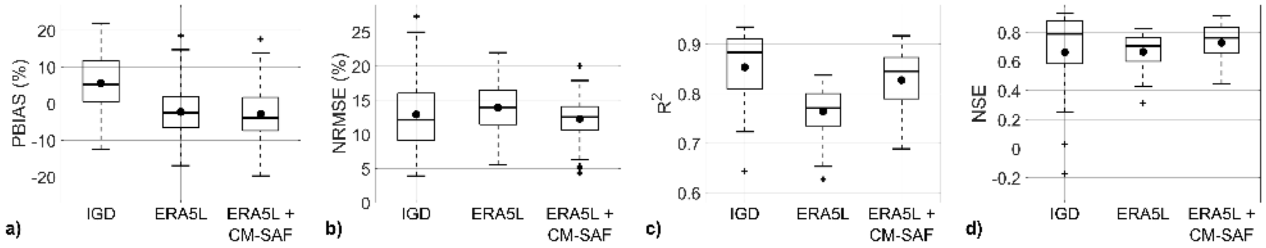

Fig. 9. Statistical indices of daily ET_o at 38 AWS sites (validation set)

These results are in agreement with a similar study conducted in another region of southern Italy for which the mean NRMSE of the PM-ET$_o$ estimates computed with ERA5L data was 17%, while it was 22% with the former UERRA regional reanalysis forced by ERA-Interim (Pelosi et al., 2020a). Neither performance in the above study was far from those obtained by kriging interpolation, which presented the same average NRMSE of 14%.

Table 5 shows the NRMSE with a monthly aggregation for the three scenarios: ERA5L+CM-SAF always outperforms the others especially in April, May and September when the overall performances are slightly worst due to the more possible presence of weather instabilities. The ET$_o$ in June, July and August are better described by all three methods than in the remaining months.

Table 5. Monthly NRMSE according to the three scenarios summarized in Table 3.

		APR	**MAY**	**JUN**	**JUL**	**AUG**	**SEP**
NRMSE (%)	**IGD**	14	13	12	12	13	14
	ERA5L	16	15	13	12	13	16
	ERA5L + CM-SAF	13	12	11	11	12	14

Fig. 10 shows the regional spatial variability of mean PBIAS and NRMSE computed with the validation sets at the AWS sites. These indices do not replicate any spatial trend, since they are the outcomes of multiple weather variables processed through a nonlinear model such as the FAO Penman-Monteith equation. However, ET$_o$ estimates tend to be less accurate in mountainous areas, similarly to what was observed for R$_s$ in Fig. 8 and on the coast. In addition, those sites with large errors in wind speed estimates are also subject to major errors in ET$_o$ estimates.

This is a post-peer-review, pre-copyedit version of an article published in *Agricultural Water Management*.
The final authenticated version is available online at: ***https://doi.org/10.1016/j.agwat.2021.107169***

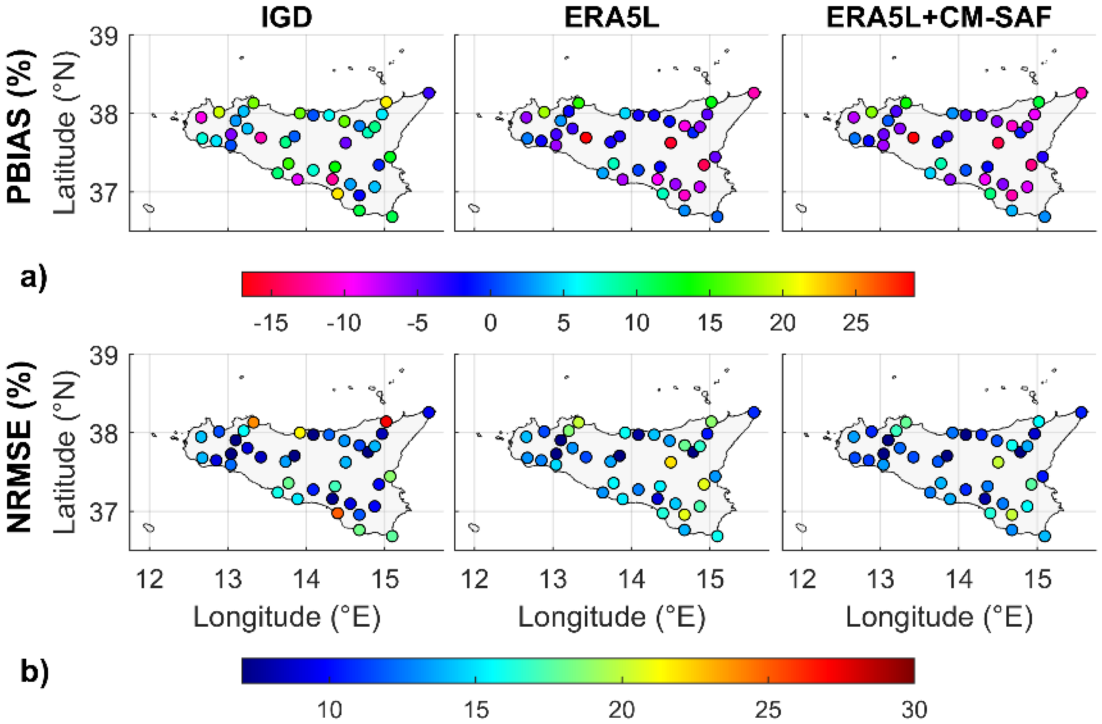

Fig. 10. Spatial depiction of the statistical indices PBIAS and NRMSE computed at the AWS sites, averaged over the validation set and related to the three different datasets of daily reference evapotranspiration computed, respectively, by means of (i) spatial interpolated ground-based data (IGD), (ii) bias-corrected ERA5-Land data and (iii) ERA5-Land data combined with bias-corrected CM-SAF radiation data

ERA5L+CM-SAF ET_o estimates outperform ERA5L ET_o estimates everywhere in the region, especially in terms of NRMSE, R^2 and NSE due to the better performance of CM-SAF R_s products in comparison with ERA5L R_s, as shown above. However, the impact of the improvements using the ERA5L+CM-SAF method rather than ERA5L is less than expected judging from the performance of CM-SAF radiation products in comparison with ERA5L (Section 4.1.4). This is mainly due to the slight sensitivity of ET_o to the differences between ERA5-Land and CMS-SAF solar radiation data as illustrated in Figs. 11a-b, which show that the PBIAS and NRMSE of the ET_o estimates computed with ground-based weather variables change after substituting one at a time a ground-based weather variable with the respective reanalysis or satellite-based estimation (as indicated on the x-axis).

This is a post-peer-review, pre-copyedit version of an article published in *Agricultural Water Management*.
The final authenticated version is available online at: *https://doi.org/10.1016/j.agwat.2021.107169*

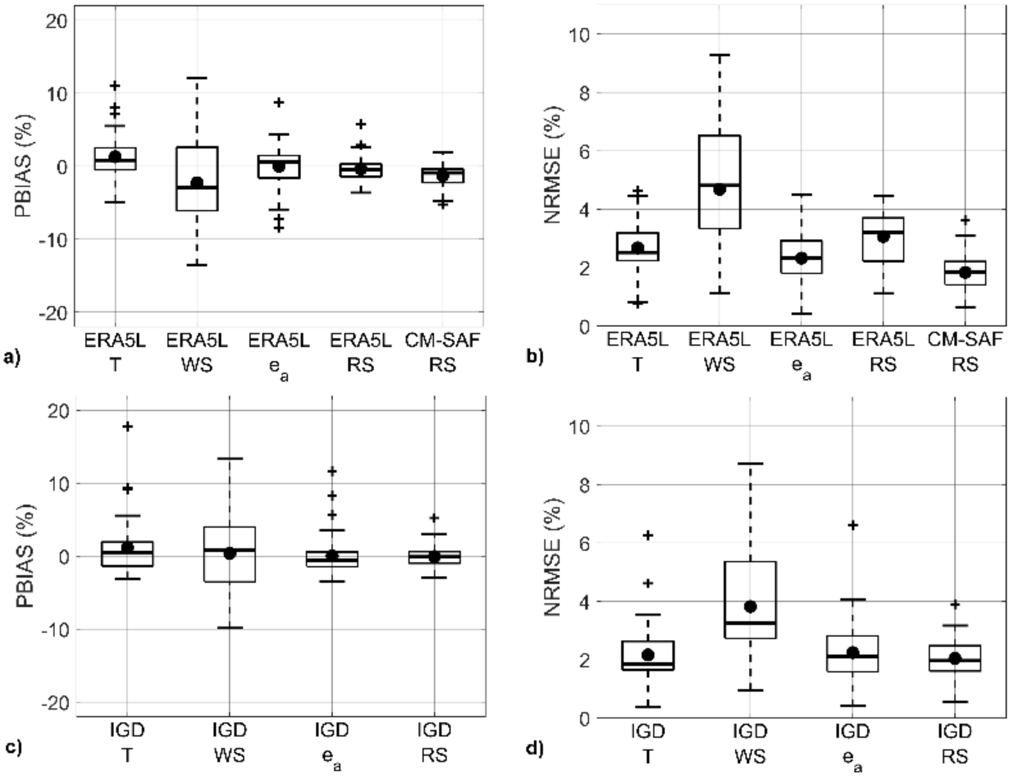

Fig. 11. Sensitivity of the daily FAO Penman-Monteith ET_o estimates to errors in reanalysis weather variables and satellite-based products. The five ET_o estimates are obtained by using ground-based data except for the variable indicated on the x-axis that was retrieved from either IGD or ERA5L or CM-SAF.

Fig. 11a confirms that by using all observed weather variables except ERA5L radiation, the mean NRMSE increases by almost 3% (about 0.2 mm day^{-1}). By using all observed weather variables except CM-SAF radiation, the mean NRMSE increases by almost 2% (about 0.1 mm day^{-1}). Similar results were obtained by Paredes et al. (2021), who proposed the use of a satellite-based radiation product instead of ground measurements and ERA5 radiation products. In their study for continental Portugal, the mean RMSE of the ET_o estimates decreased by 0.2 mm day^{-1} when LSA-SAF radiation was used instead of ERA5 radiation. Here, by using CM-SAF R_s instead of ERA5-Land R_s, RMSE decreased by 0.1 mm day^{-1}; this smaller difference in RMSE with respect to Paredes et al. (2021) is due to ERA5-Land outperforming ERA5.

Moreover, Figs. 11 show that the largest errors in ET_o estimates are obtained when wind speed ground data are changed with IGD or ERA5L wind data. ET_o errors with IGD R_s are similar to those obtained with CM-SAF R_s, analogously ET_o errors with IGD temperature are similar to those obtained with ERA5L temperature, in accordance with the results presented in Section 4.1.1.

5. Conclusions

Remote sensing and reanalysis products represent important data sources for regional assessment of the hydrological variables relevant to water resource planning and climate studies. However, proper regional scale analyses must be implemented to evaluate their added value with respect to what could be achieved by spatially interpolating sparse ground observations. In this study, a cross validation procedure, consisting in recursively interpolating data by universal kriging and ordinary kriging, was adopted to evaluate the performance of a regional spatial interpolation.

This study confirmed that satellite-based solar radiation data delivered by CM-SAF can be effectively employed for water resources management applications, especially in those regions where it is difficult to gather weather data recorded by ground weather stations.

In the examined region, served by a relatively dense network of ground weather stations, bias-corrected solar radiation estimates provided by CM-SAF outperformed those estimates obtained by spatially interpolating solar radiation data recorded by the pyranometers at the ground weather stations.

Performance indicators of ET_o estimates computed with a weather dataset consisting of CM-SAF solar radiation data and ERA5-Land weather data are comparable to those computed with spatially interpolated weather data. Ground weather observations are still fundamental for bias-correcting remotely sensed data. However, a relatively short time series is sufficient to achieve valid bias correction (in this study, six irrigation seasons out of 18).

These results confirm the hypothesis that an optimal blending of reanalysis and satellite-based data can be used with high accuracy and confidence for the regional assessment of ET_o, when ground

This is a post-peer-review, pre-copyedit version of an article published in *Agricultural Water Management*.
The final authenticated version is available online at: ***https://doi.org/10.1016/j.agwat.2021.107169***

weather data cannot be easily gathered due to the inaccessibility and lack of interoperability of ground-based weather databases. Moreover, it might be even better to use CM-SAF blended with ERA5-Land for the assessment of ET_o in regions where the spatial interpolation of ground weather data is prone to large uncertainties due to the poor spatial distribution and density of the weather sensors, as very often occurs for pyranometers.

Declaration of Competing Interest

The authors declare that they have no known competing financial interests or personal relationships that could have appeared to influence the work reported in this paper.

Acknowledgements

Satellite solar radiation products are made available by the EUMETSAT Satellite Applications Facility on Climate Monitoring (www.cmsaf.eu). The ERA5-Land reanalysis data are Copernicus products belonging to European Union and accessible on the ECMWF Copernicus Climate Data Store (CDS - https://cds.climate.copernicus.eu). Ground weather data were provided by SIAS regional service (http://www.sias.regione.sicilia.it). The authors gratefully acknowledge the two anonymous Reviewers and the Associate Editor Dr. Paula Paredes for the constructive comments and suggestions.

Appendix A. Statistics of the reference automatic weather stations

Table A1 Main statistics of the selected automatic weather stations in Sicily

No.	Name	Elevation (m)	Longitude (°E)	Latitude (°N)	T_{max} (°C)	T_{min} (°C)	Rs (W m^{-2})	e_a (kPa)	u_{10} (m s^{-1})
1	Agrigento	40	13° 38’ 09’’	37° 14’ 16’’	26.2	16.9	275	1.6	2.9
2	Cammarata	379	13° 44’ 11’’	37° 37’ 55’	28.5	12.8	263	1.3	2.2
3	Canicattì	475	13° 46’ 24’’	37° 21’ 30’’	27.7	14.0	260	1.3	2.1
4	Licata	80	13° 53’ 20’’	37° 09’ 20’’	28.1	18.0	275	1.5	3.6
5	Sciacca	90	13° 02’ 23’’	37° 35’ 30’’	28.6	17.0	275	1.4	2.9
6	Gela	70	14° 20° 01’’	37° 09’ 32’’	29.2	15.1	272	1.4	2.9
7	Riesi	300	14° 05’ 21’’	37° 16’ 32’’	28.7	16.0	260	1.4	2.2
8	Sclafani Bagni	497	13° 51’ 00’’	37° 42’ 21’’	28.0	13.0	266	1.2	1.6
9	Bronte	424	14° 47’ 13’’	37° 45’ 18’’	29.1	13.7	251	1.2	1.5
10	Catania	10	15° 04’ 08’’	37° 26’ 26’’	27.9	16.9	266	1.5	2.2
11	Maletto	1040	14° 52’ 23’’	37° 49’ 39’’	23.3	13.4	252	1.1	2.1
12	Mazzarrone	300	14° 33’ 42’’	37° 05’ 45’’	28.3	15.2	268	1.3	2.5
13	Piazza Armerina	540	14° 21’ 59’’	37° 19’ 02’’	27.4	14.9	264	1.3	2.3
14	Caronia	1470	14° 29’ 11’’	37° 53’ 48’’	17.9	10.1	252	1.0	3.8
15	Cesarò	820	14° 40’ 47’’	37° 50’ 19’’	24.9	13.8	254	1.1	2.2
16	Messina	420	15° 33’ 40’’	38° 15’ 31’’	23.5	16.7	263	1.6	3.8
17	Patti	88	15° 01’ 10’’	38° 08’ 28’’	27.0	16.3	257	1.6	1.2
18	Pettineo	210	14° 17’ 00’’	37° 58’ 27’’	26.4	17.3	259	1.5	2.1
19	Camporeale	460	13° 06’ 03’’	37° 54’ 18’’	26.2	16.1	263	1.4	2.3
20	Castelbuono	430	14° 05’ 23’’	37° 58’ 29’’	25.3	16.7	264	1.4	2.2
21	Contessa Entellina	200	13° 02’ 36’’	37° 43’ 50’’	29.4	15.4	268	1.4	2.6
22	Corleone	450	13° 15’ 02’’	37° 48’ 17’’	27.8	15.6	265	1.3	2.4
23	Lascari	55	13° 55’ 12’’	38° 00’ 00’’	27.5	17.1	259	1.6	1.8
24	Monreale	612	13° 12’ 11’’	38° 01’ 32’’	25.2	14.1	259	1.3	2.6
25	Palermo	50	13° 19’ 40’’	38° 07’ 51’’	27.4	18.5	256	1.5	1.5
26	Acate	60	14° 24’ 02’’	36° 58’ 30’’	27.1	16.5	272	1.7	2.2
27	Ragusa	705	14° 40’ 37’’	36° 57’ 20’’	24.5	15.7	272	1.3	3.9
28	Scicli	51	14° 40’ 36’’	36° 45’ 40’’	26.8	17.6	269	1.7	2.8
29	Lentini	50	14° 55’ 32’’	37° 20’ 32’’	30.1	16.6	265	1.4	3.0
30	Pachino	50	15° 05’ 43’’	36° 40’ 57’’	26.4	18.2	279	1.8	3.2
31	Palazzolo Acreide	640	14° 52’ 18’’	37° 03’ 43’’	26.6	15.8	260	1.3	2.8
32	Castellammare del Golfo	90	12° 53’ 22’’	38° 00’ 52’’	26.8	16.9	250	1.7	1.9
33	Castelvetrano	120	12° 51’ 10’’	37° 38’ 52’’	28.1	15.5	271	1.4	2.7
34	Mazara del Vallo	30	12° 40’ 30’’	37° 40’ 47’’	28.5	14.9	269	1.5	2.8
35	Trapani	180	12° 39’ 41’’	37° 56’ 51’’	27.4	17.1	266	1.5	3.8
36	Montalbano Elicona	1250	14° 58’ 00’’	37° 59’ 10’’	19.8	11.4	238	1.1	3.4
37	Prizzi	1124	13° 25’ 18’’	37° 41’ 20’’	22.8	13.4	257	1.1	3.4
38	Agira	467	14° 30’ 07’’	37° 37’ 24’’	28.3	16.3	262	1.2	2.8

This is a post-peer-review, pre-copyedit version of an article published in *Agricultural Water Management*.
The final authenticated version is available online at: *https://doi.org/10.1016/j.agwat.2021.107169*

Appendix B. Ordinary and regression kriging

In geostatistical methods, the variable of interest is considered as a random function of the space **x**, Z(**x**), and the set of observed values at the *m* sampling locations {z(**x**$_1$), z(**x**$_2$), …, z(**x**$_m$)}, represents one realization of this random function. The kriging interpolator allows the predicted value of the variable of interest at an ungauged location, **x**$_k$, to be expressed as a linear combination of {Z(**x**$_1$), Z(**x**$_2$), …, Z(**x**$_m$)} as follows:

$$\hat{\mathrm{Z}}(\mathbf{x_k}) = \sum_{\mathrm{i}=1}^{\mathrm{m}} w_{\mathrm{i}}\, \mathrm{Z}(\mathbf{x_i}) \qquad \text{(B.1)}$$

where the weights w_i, for i= 1, …m, are obtained by solving the kriging system that provides the optimal, with minimum variance criterion, unbiased linear estimator (BLUE – Best Linear Unbiased Estimator).

Ordinary kriging assumes the hypothesis of constant unknown mean, μ, over the search neighborhood of **x**$_k$. The ordinary kriging system can be written as follows:

$$\begin{cases} \sum_{j=1}^{m} w_{\mathrm{j}}\, \gamma_Z\left(\left\|\mathbf{x_i}-\mathbf{x_j}\right\|\right) - \mu = \gamma_Z\left(\|\mathbf{x_i}-\mathbf{x}\|\right) \quad \text{for } i=1,\dots,m \\ \sum_{j=1}^{m} w_j = 1 \end{cases} \qquad \text{(B.2)}$$

where γ is the semi-variogram of the random field, Z(**x**).

Under the hypothesis of an intrinsically stationary, isotropic random field Z(**x**), the semi-variogram unambiguously describes the spatial autocorrelation of the sampling locations and it can be estimated from data (i.e., experimental semi-variogram) as follows:

$$\hat{\gamma}_Z(\mathrm{h}) = \frac{1}{2}\mathrm{E}[\mathrm{Z}(\mathbf{x}+h) - \mathrm{Z}(\mathbf{x})]^2 \qquad \text{(B.3)}$$

where *h* is the varying distance (lag) between two sampling locations. Then, by fitting the experimental semi-variogram with a suitable parametric analytic function, the theoretical semi-variogram of the field, γ_Z is defined. Among various analytical functions used to fit the experimental semi-variograms, the exponential curve is here employed:

$$\gamma_Z(h) = n_g + s\left[1 - \exp\left(-\frac{h}{r}\right)\right] \qquad \text{(B.4)}$$

This is a post-peer-review, pre-copyedit version of an article published in *Agricultural Water Management*.
The final authenticated version is available online at: *https://doi.org/10.1016/j.agwat.2021.107169*

where h is the varying lag distance; n_g, r and s are parameters of the curve called nugget, partial sill and range, respectively. The nugget is the value of the semi-variogram at lag equal to zero and it is theoretically zero. However, in the presence of small-scale variability and/or measurements errors, the nugget is not zero (nugget effect). The range defines the distance within the sample locations are spatially correlated. The value reached by the semi-variogram model at a lag equal to the range is called the sill. The partial sill is the sill minus the nugget.

For the regression kriging, a regression analysis is first carried out between the variable of interest and an auxiliary variable, y ($\mathbf{x}$):

$$Z^{*}(\mathbf{x}) = a\, y(\mathbf{x}) + b \qquad \text{(B.5)}$$

where Z*(x) is the fitted value of the variable of interest and a and b are the regression coefficients estimated by the OLS method. The kriging estimator of Eqs. (B.1-B.6) is then applied to the regression residuals, $r(\mathbf{x}) = Z^{*}(\mathbf{x}) - \mathrm{Z}(\mathbf{x})$, to obtain the prediction of the residual at the unsampled location $\mathbf{x_k}$, $\hat{r}(\mathbf{x_k})$ and hence the predicted value of the variable of interest $\hat{\mathrm{Z}}(\mathbf{x_k})$ as follows:

$$\hat{\mathrm{Z}}(\mathbf{x_k}) = Z^{*}(\mathbf{x_k}) - \hat{\mathrm{r}}(\mathbf{x_k}) \qquad \text{(B.6)}$$

This is a post-peer-review, pre-copyedit version of an article published in *Agricultural Water Management*.
The final authenticated version is available online at: *https://doi.org/10.1016/j.agwat.2021.107169*

Appendix C. Performance statistics of daily weather variables before and after bias correction

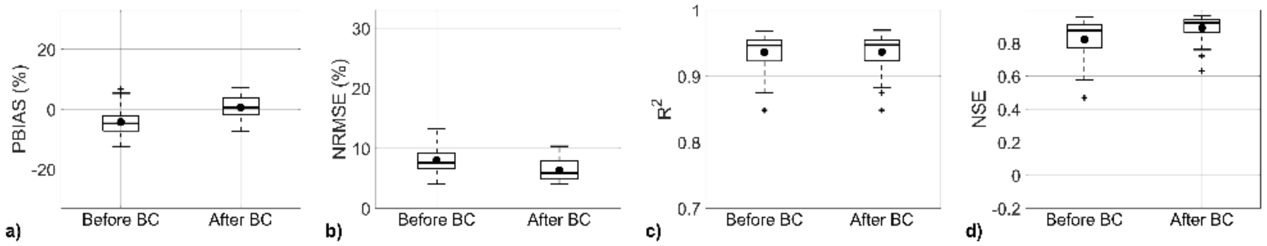

Fig. C1. Statistical indices of daily T_{max} for all 38 AWS sites before and after regional mean bias correction

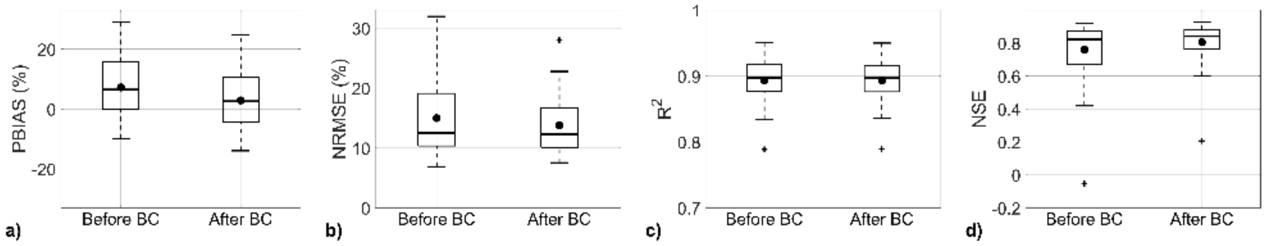

Fig. C2. Statistical indices of daily T_{min} for all 38 AWS sites before and after regional mean bias correction

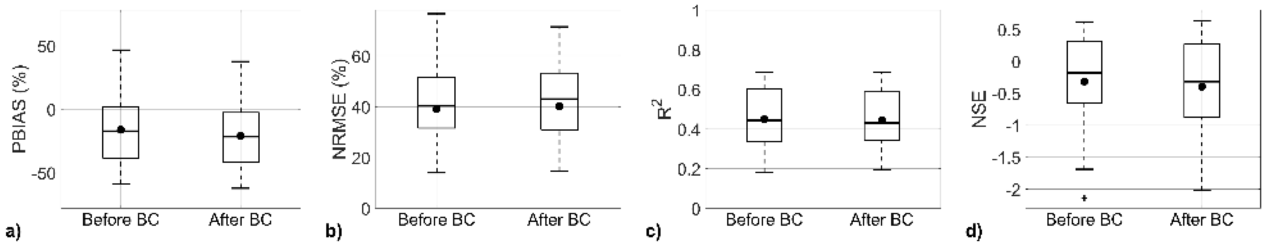

Fig. C3. Statistical indices of daily u_{10} for all 38 AWS sites before and after regional mean bias correction

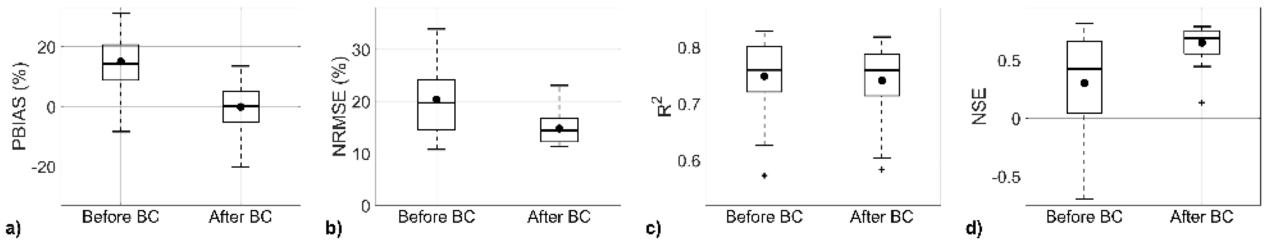

Fig. C4. Statistical indices of daily e_a for all 38 AWS sites before and after regional mean bias correction

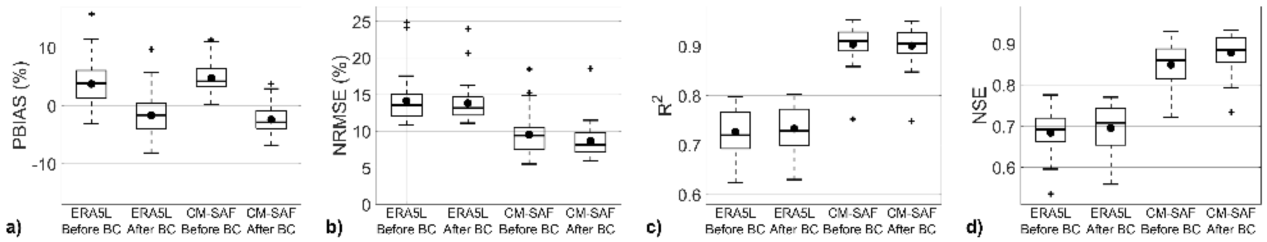

Fig. C5. Statistical indices of daily R_s for all 38 AWS sites before and after regional mean bias correction

This is a post-peer-review, pre-copyedit version of an article published in *Agricultural Water Management*.
The final authenticated version is available online at: ***https://doi.org/10.1016/j.agwat.2021.107169***

References

Ahmed, S., de Marsily, G., 1987. Comparison of geostatistical methods for estimating transmissivity using data on transmissivity and specific capacity. Water Resour. Res. 23, 1717–1737. https://doi.org/10.1029/WR023i009p01717.

Allen, R.G., 1996. Assessing integrity of weather data for use in reference evapotranspiration estimation. Journal of Irrigation and Drainage Engineering 122(2), 97-106. https://doi.org/10.1061/(ASCE)0733-9437(1996)122:2(97)

Allen, R.G., 2000. Using the FAO-56 dual crop coefficient method over an irrigated region as part of an evapotranspiration intercomparison study. J. Hydrol. 229, 27–41. https://doi.org/10.1016/S0022-1694(99)00194-8.

Allen, R.G., Pereira, L.S., Raes, D., Smith, M., 1998. Crop Evapotranspiration. Guidelines for Computing Crop Water Requirements, FAO Irrigation and Drainage Paper 56. FAO, Rome, p. 300. Paper 56.

Alsamamra, H., Ruiz-Arias, J.A., Pozo-Vazquez, D., Tovar-Pescador, J., 2009. A comparative study of ordinary and residual kriging techniques for mapping global solar radiation over southern Spain. Agric. For. Meteorol. 149, 1343–1357. https://doi.org/10.1016/j.agrformet.2009.03.005.

Battisti, R, Bender, F.D., Sentelhas, P.C., 2019. Assessment of different gridded weather data for soybean yield simulations in Brazil. Theor. Appl. Climatol. 135, 237–247. https://doi.org/10.1007/s00704-018-2383-y.

Bauer, P., Thorpe, A., Brunet, G., 2015. The quiet revolution of numerical weather prediction. Nature 525, 47–55. https://doi:10.1038/nature14956.

Berndt, C., Haberlandt, U., 2018. Spatial interpolation of climate variables in Northern Germany—Influence of temporal resolution and network density. J. Hydrol. Reg. Stud. 15, 184–202. https://doi.org/10.1016/j.ejrh.2018.02.002.

Boulard, D., Castel, T., Camberlin, P., Sergent, A.-S., Br´eda, N., Badeau, V., Rossi, A., Pohl, B., 2016. Capability of a regional climate model to simulate climate variables requested for water balance computation: a case study over northeastern France. Clim. Dyn. 46, 2689–2716. https://doi.org/10.1007/s00382-015-2724-9.

Calera, A., Campos, I., Osann, A., D'Urso, G., Menenti, M., 2017. Remote Sensing for Crop Water Management: From ET Modelling to Services for the End Users. Sensors 17, 1104. https://doi.org/10.3390/s17051104.

Cammalleri, C., Ciraolo, G., 2013. A simple method to directly retrieve reference evapotranspiration from geostationary satellite images. Int. J. Appl. Earth Obs. Geoinf. 21, 149–158. https://doi.org/10.1016/j.jag.2012.08.008.

Cammalleri, C., Ciraolo, G., La Loggia, G., Maltese, A., 2012. Daily evapotranspiration assessment by means of residual surface energy balance modeling: A critical analysis under a wide range of water availability. J. Hydrol. 452–453, 119-129. https://doi.org/10.1016/j.jhydrol.2012.05.042.

Chirico, G.B., Pelosi, A., De Michele, C., Falanga Bolognesi, S., D'Urso, G., 2018. Forecasting potential evapotranspiration by combining numerical weather predictions and visible and near-infrared satellite images: An application in southern Italy. J. Agric. Sci. 156, 702–710. https://doi:10.1017/S0021859618000084.

Chirico, G.B., Medina, H., Romano, N., 2010. Functional evaluation of PTF prediction uncertainty: An application at hillslope scale. Geoderma 155, 193–202. https://doi.org/10.1016/j.geoderma.2009.06.008.

Consoli, S., Vanella, D., 2014. Mapping crop evapotranspiration by integrating vegetation indices into a soil water balance model. Agric. Water Manag. 143, 71-81. https://doi.org/10.1016/j.agwat.2014.06.012.

Cressie, N., 1993. Statistics for Spatial Data. John Wiley and Sons, New York, NY, USA.

Cristóbal, J., Anderson, M.C., 2013. Validation of a Meteosat second generation solar radiation dataset over the northeastern Iberian Peninsula. Hydrol. Earth Syst. Sci. 17 (1), 163–175. https://doi.org/10.5194/hess-17-163-2013.

Cruz-Blanco, M., Gavilán, P., Santos, C., Lorite, I.J., 2014. Assessment of reference evapotranspiration using remote sensing and forecasting tools under semi-arid conditions. Int. J. Appl. Earth Obs. 33, 280–289. https://doi.org/10.1016/j.jag.2014.06.008.

This is a post-peer-review, pre-copyedit version of an article published in *Agricultural Water Management*.
The final authenticated version is available online at: *https://doi.org/10.1016/j.agwat.2021.107169*

Di Piazza, A., Lo Conti, F., Viola, F., Eccel, E., Noto, L.V., 2015. Comparative Analysis of Spatial Interpolation Methods in the Mediterranean Area: Application to Temperature in Sicily. Water 7, 1866–1888. https://doi.org/10.3390/w7051866.

Dutra, E., Muñoz Sabater, J., Boussetta, S., Komori, T., Hirahara, S., Balsamo, G., 2020. Environmental lapse rate for high-resolution land surface downscaling: An application to ERA5. Earth and Space Sci. 7, e2019EA000984. https://doi.org/10.1029/2019EA000984.

European Parliament, 2013. Regulation (EU) No 1305/2013 of the European Parliament and of the Council of 17 December 2013 on support for rural development by the European Agricultural Fund for Rural Development (EAFRD) and repealing Council Regulation (EC) No 1698/2005. Official Journal of the European Union, L 347/487. http://data.europa.eu/eli/reg/2013/1305/oj.

Furcolo, P., Pelosi, A., Rossi, F., 2016. Statistical identification of orographic effects in the regional analysis of extreme rainfall. Hydrol. Process. 30, 1342–1353, https://doi:10.1002/hyp.10719.

Gao, L., Bernhardt, M., and Schulz, K., 2012. Elevation correction of ERA-Interim temperature data in complex terrain. Hydrol. Earth Syst. Sci. 16, 4661–4673. https://doi.org/10.5194/hess-16-4661-2012.

González-Dugo, M.P., Neale, C.M.U., Mateos, L., Kustas, W.P., Prueger, J.H., Anderson, M.C., Li, F., 2009. A comparison of operational remote sensing-based models for estimating crop evapotranspiration. Agric. For. Meteorol. 149, 1843–1853. https://doi.org/10.1016/j.agrformet.2009.06.012.

Gupta, A.S., Tarboton, D. G., 2016. A tool for downscaling weather data from large-grid reanalysis products to finer spatial scales for distributed hydrological applications. Environ. Model. Softw. 84, 50-69. https://doi.org/10.1016/j.envsoft.2016.06.014.

Hersbach, H, Bell, B, Berrisford, P, et al. The ERA5 global reanalysis. Q J R Meteorol Soc. 2020 146, 1999– 2049. https://doi.org/10.1002/qj.3803

Hofstra, N., Haylock, M., New, M., Jones, P., Frei, C., 2008. Comparison of six methods for the interpolation of daily, European climate data. J. Geophys. Res. Atmos. 113, D21110. https://doi.org/10.1029/2008JD010100.

Holdaway, M.R., 1996. Spatial modelling and interpolation of monthly temperature using kriging. Clim. Res. 6, 215–225.

This is a post-peer-review, pre-copyedit version of an article published in *Agricultural Water Management*.
The final authenticated version is available online at: *https://doi.org/10.1016/j.agwat.2021.107169*

Iglesias, A., Garrote, L., 2015. Adaptation strategies for agricultural water management under climate change in Europe. Agric. Water Manag. 155, 113-124. https://doi.org/10.1016/j.agwat.2015.03.014.

Jarvis, C.H., Stuart, N., 2001. A comparison among strategies of interpolating maximum and minimum daily air temperatures. Part I: The selection of "guiding" topographic and land cover variables. J. Appl. Meteorol. 40, 1060–1074. https://doi.org/10.1175/1520-0450(2001)040<1075:ACASFI>2.0.CO;2.

Journée, M., Bertrand, C., 2010. Improving the spatio-temporal distribution of surface radiation data by merging ground and satellite measurements. Remote Sens. Environ. 114 (11), 2692–2704. https://doi.org/10.1016/j.rse.2010.06.010.

Journel, A.G., Huijbregts, C.J., 1978. Mining Geostatistics. Academic Press, London, UK.

Jung, C.G., Lee, D.R., Moon, J.W., 2016. Comparison of the Penman-Monteith method and regional calibration of the Hargreaves equation for actual evapotranspiration using SWAT-simulated results in the Seolma-cheon basin, South Korea. Hydrol. Sci. J. 61, 793–800. https://doi.org/10.1080/02626667.2014.943231.

Krause, P., Boyle, D. P., Bäse, F., 2005. Comparison of different efficiency criteria for hydrological model assessment, Adv. Geosci. 5, 89–97, https://doi.org/10.5194/adgeo-5-89-2005.

Lee, D.T., Schachter, B.J., 1980. Two algorithms for constructing a Delaunay triangulation. Internat. Comput. Inform. Sci. 9, 219–242.

Lewis, C.S., Geli, H.M.E., Neale, C.M.U., 2014. Comparison of the NLDAS weather forcing model to agrometeorological measurements in the western United States. J. Hydrol. 510, 385–392. https://doi.org/10.1016/j.jhydrol.2013.12.040.

Liuzzo, L., Bono, E., Sammartano, V., Freni, G., 2017. Long-term temperature changes in Sicily, Southern Italy. Atmos. Res. 198, 44-55, https://doi.org/10.1016/j.atmosres.2017.08.007.

Llop, M., Ponce-Alifonso, X., 2016. Water and Agriculture in a Mediterranean Region: The Search for a Sustainable Water Policy Strategy. Water 8, 66. https://doi.org/10.3390/w8020066.

Longo-Minnolo, G., Vanella, D., Consoli, S., Intrigliolo, D.S., Ramírez-Cuestac, J.M., 2020. Integrating forecast meteorological data into the ArcDualKc model for estimating spatially distributed evapotranspiration rates of a citrus orchard. Agric. Water Manag. 231, 105967. https://doi.org/10.1016/j.agwat.2019.105967.

Luo, W., Taylor, M.C., Parker, S.R., 2008. A comparison of spatial interpolation methods to estimate continuous wind speed surfaces using irregularly distributed data from England and Wales. Int. J. Clim. 28, 947–959. https://doi.org/10.1002/joc.1583.

Martins, D.S., Paredes, P., Raziei, T., Pires, C., Cadima, J., Pereira, L.S., 2017. Assessing reference evapotranspiration estimation from reanalysis weather products. An application to the Iberian Peninsula. Int. J. Climatol. 37, 2378–2397. https://doi.org/10.1002/joc.4852 .

Medina, H., Tian, D., Srivastava, P., Pelosi, A., Chirico, G.B., 2018. Medium-range reference evapotranspiration forecasts for the contiguous United States based on multi-model numerical weather predictions. J. Hydrol. 562, 502–517, https://doi:10.1016/j.jhydrol.2018.05.029.

Moore, F., Lobell, D. 2014. Adaptation potential of European agriculture in response to climate change. Nature Clim Change 4, 610–614. https://doi.org/10.1038/nclimate2228.

Mueller, R., Behrendt, T., Hammer, A., Kemper, A., 2012. A New Algorithm for the Satellite-Based Retrieval of Solar Surface Irradiance in Spectral Bands. Remote Sens. 4, 622-647. https://doi.org/10.3390/rs4030622.

Mueller, R.W., Matsoukas, C., Gratzki, A., Behr, H.D., Hollmann, R., 2009. The CM SAF operational scheme for the satellite-based retrieval of solar surface irradiance – A LUT based eigenvector approach, Remote Sens. Environ. 113, 1012-1024. https://doi.org/10.1016/j.rse.2009.01.012.

Muñoz Sabater, J., 2019. ERA5-Land hourly data from 1981 to present. Copernicus Climate Change Service (C3S) Climate Data Store (CDS). (Accessed on 18 July 2020), https://doi:10.24381/cds.e2161bac.

Odeh, I.O.A., McBratney, A.B., Chittleborough, D.J., 1995. Further results on prediction of soil properties from terrain attributes: Heterotopic cokriging and regression-kriging. Geoderma 67, 215–226. https://doi.org/10.1016/0016-7061(95)00007-B.

Ohmura, A., et al., 1998. Baseline Surface Radiation Network (BSRN/WCRP): New precision radiometry for climate research. Bull. Amer. Meteor. Soc. 79, 2115-2136.

This is a post-peer-review, pre-copyedit version of an article published in *Agricultural Water Management*.
The final authenticated version is available online at: *https://doi.org/10.1016/j.agwat.2021.107169*

Paredes, P., Martins, D.S., Pereira, L.S., Cadima, J., Pires, C., 2018. Accuracy of daily estimation of grass reference evapotranspiration using ERA-Interim reanalysis products with assessment of alternative bias correction schemes. Agric. Water Manag. 210, 340–353. https://doi.org/10.1016/j.agwat.2018.08.003.

Paredes, P., Pereira, L.S., Almorox, J., Darouich, H., 2020. Consolidated methods to compute reference grass evapotranspiration with reduced data sets by parameterizing the FAO Penman-Monteith temperature approach and the Hargeaves-Samani equation using regional climatic variables. Agric. Water Manag. 240, 106210 https://doi.org/10.1016/j.agwat.2020.106210.

Paredes, P., Trigo, I., de Bruin, H., Simões, N., Pereira, L.S., 2021. Daily grass reference evapotranspiration with Meteosat Second Generation shortwave radiation and reference ET products. Agric. Water Manag. 248, 106543. https://doi.org/10.1016/j.agwat.2020.106543.

Peel, M. C., Finlayson, B. L. and McMahon, T. A., 2007. Updated world map of the Köppen–Geiger climate classification. Hydrol. Earth Syst. Sci. 11: 1633–1644. https://doi:10.5194/hess-11-1633-2007.

Pelosi, A., Furcolo, P., 2015. An amplification model for the regional estimation of extreme rainfall within orographic areas in Campania region (Italy). Water 7, 6877–6891, https://doi:10.3390/w7126664.

Pelosi, A., Medina, H., Van den Bergh, J., Vannitsem, S., Chirico, G.B., 2017. Adaptive Kalman filtering for post-processing of ensemble numerical weather predictions. Mon. Weather Rev. 145, 4837–4854. https://doi:10.1175/MWR-D-17-0084.1.

Pelosi, A., Medina, H., Villani, P., D'Urso, G., Chirico, G.B., 2016. Probabilistic forecasting of reference evapotranspiration with a limited area ensemble prediction system. Agric. Water Manag. 178, 106–118, https://doi:10.1016/j.agwat.2016.09.015.

Pelosi, A., Terribile, F., D'Urso, G., Battista Chirico, G., 2020a. Comparison of ERA5-Land and UERRA MESCAN-SURFEX reanalysis data with spatially interpolated weather observations for the regional assessment of reference evapotranspiration. Water 12, 1669. https://doi.org/10.3390/w12061669.

This is a post-peer-review, pre-copyedit version of an article published in *Agricultural Water Management*.
The final authenticated version is available online at: *https://doi.org/10.1016/j.agwat.2021.107169*

Pelosi, A., Villani, P., Falanga Bolognesi, S., Chirico, G.B., D'Urso, G., 2020b. Predicting Crop Evapotranspiration by Integrating Ground and Remote Sensors with Air Temperature Forecasts. Sensors 20, 1740. https://doi.org/10.3390/s20061740.

Pereira, A.R., 2004. The Priestley–Taylor parameter and the decoupling factor for estimating reference evapotranspiration. Agric. For. Meteorol. 194, 50–63. https://doi.org/10.1016/j.agrformet.2004.04.002.

Pereira, L.S., 2017. Water, agriculture, and food: challenges and issues. Water Resour. Manag. 31, 2985–2999. https://doi.org/10.1007/s11269-017-1664-z.

Pereira, L.S., Cordery, I., Iacovides, I., 2012. Improved indicators of water use performance and productivity for sustainable water conservation and saving. Agric. Water Manag. 108, 39–51. https://doi.org/10.1016/j.agwat.2011.08.022.

Perera, K.C., Western, A.W., Nawarathna, B., George, B., 2014. Forecasting daily reference evapotranspiration for Australia using numerical weather prediction outputs. Agric. For. Meteorol. 125, 305–313. https://doi.org/10.1016/j.agrformet.2014.03.014.

Pfeifroth, Uwe, Trentmann, Jörg, Hollmann, Rainer, Selbach, Nathalie, Werscheck, Martin, Meirink, Jan Fokke, 2018. ICDR SEVIRI Radiation - based on SARAH-2 methods, Satellite Application Facility on Climate Monitoring. (Accessed on 04 January 2021). https://wui.cmsaf.eu/safira/action/viewICDRDetails?acronym=SARAHV002ICDR.

Prudhomme, C., Reed, D., 1999. Mapping extreme rainfall in a mountainous region using geostatistical techniques: A case study in Scotland. Int. J. Climatol. 19, 1337–1356.

Rehman, S., Ghori, S.G., 2000. Spatial estimation of global solar radiation using geostatistics. Renew. Energy 21, 583–605. https://doi.org/10.1016/S0960-1481(00)00078-1.

Ren, X., Qu, Z., Martins, D.S., Paredes, P., Pereira, L.S., 2016. Daily reference evapotranspiration for hyper-arid to moist sub-humid climates in Inner Mongolia, China: I. Assessing temperature methods and spatial variability. Water Resour. Manag. 30, 3769–3791. https://doi.org/10.1007/s11269-016-1384-9.

Ricard, S., Anctil, F., 2019. Forcing the Penman-Monteith Formulation with Humidity, Radiation, and Wind Speed Taken from Reanalysis, for Hydrologic Modeling. Water 11, 1214. https://doi.org/10.3390/w11061214.

This is a post-peer-review, pre-copyedit version of an article published in *Agricultural Water Management*.
The final authenticated version is available online at: *https://doi.org/10.1016/j.agwat.2021.107169*

Rolland, C., 2003. Spatial and Seasonal Variations of Air Temperature Lapse Rates in Alpine Regions. J. Clim. 16, 1032–1046.

Schmetz, J., Pili, P., Tjemkes, S., Just, D., Kerkman, J., Rota, S., Ratier, A., 2002. An introduction to Meteosat Second Generation (MSG). Bull. Am. Meteorol. Soc. 83, 977–992.

Senatore, A., Parrello, C., Almorox, J., Mendicino, G., 2020. Exploring the Potential of Temperature-Based Methods for Regionalization of Daily Reference Evapotranspiration in Two Spanish Regions. J. Irrig. Drain. Eng. 146, 05020001.

Sheridan, P., Smith, S., Brown, A., Vosper, S., 2010. A simple height-based correction for temperature downscaling in complex terrain. Met. Apps 17, 329-339. https://doi.org/10.1002/met.177.

Siebert, S. 2007. Global Map of Irrigation Areas Version 4.0.1. Food and Agriculture Organization of the United Nations (FAO), Rome, Italy. Available online: http://www.fao.org/nr/water/ aquastat/quickWMS/irrimap.htm (accessed on 21 July 2012).

Soci, C., Bazile, E., Besson, F., Landelius, T., 2016. High-resolution precipitation reanalysis system for climatological purposes. Tellus A 68, 1–19. https://doi.org/10.3402/tellusa.v68.29879.

Srivastava, P.K., Islam, T., Gupta, M., Petropoulos, G., Dai, Q., 2015. WRF dynamical downscaling and bias correction schemes for NCEP estimated hydro-meteorological variables. Water Resour. Manag. 29, 2267–2284. https://doi.org/10.1007/s11269-015-0940-z.

Stahl, K., Moore, R.D., Floyer, J.A., Asplin, M.G., McKendry, I.G., 2006. Comparison of approaches for spatial interpolation of daily air temperature in a large region with complex topography and highly variable station density. Agric. For. Meteorol. 139, 224–236. https://doi.org/10.1016/j.agrformet.2006.07.004.

Strong, C., Khatri, K.B., Kochanski, A.K., Lewis, C.S., Allen, L.N., 2017. Reference evapotranspiration from coarse-scale and dynamically downscaled data in complex terrain: Sensitivity to interpolation and resolution. J. Hydrol. 548, 406–418. https://doi.org/10.1016/j.jhydrol.2017.02.045.

Trigo, I.F., DaCamara, C.C., Viterbo, P., Roujean, J.-L., Olesen, F., Barroso, C., Camachode Coca, F., Carrer, D., Freitas, S.C., García-Haro, J., Geiger, B., Gellens- Meulenberghs, F., Ghilain,

This is a post-peer-review, pre-copyedit version of an article published in *Agricultural Water Management*.
The final authenticated version is available online at: *https://doi.org/10.1016/j.agwat.2021.107169*

N., Melía, J., Pessanha, L., Siljamo, N., Arboleda, A., 2011. The satellite application facility on land surface analysis. Int. J. Remote Sens. 32, 2725–2744. https://doi.org/10.1080/01431161003743199.

Urraca, R., Gracia-Amillo, A., Koubli, E., Huld, T., Trentmann, J., Riihelä, A., Lindfors, A., Palmer, D., Gottschalg, R., Antonanzas-Torres, F., 2017. Extensive validation of CM SAF surface radiation products over Europe. Remote Sens. Environ. 199, 171–186. https://doi.org/10.1016/j.rse.2017.07.013.

Vanella, D., Intrigliolo, D.S., Consoli, S., Longo-Minnolo, G., Lizzio, G., Dumitrache, R.C., Mateescu, E., Deelstra, J., Ramírez-Cuesta, J.M., 2020. Comparing the use of past and forecast weather data for estimating reference evapotranspiration. Agric. For. Meteorol. 295, 108196. https://doi.org/10.1016/j.agrformet.2020.108196

Vannitsem, S., 2008. Dynamical Properties of MOS Forecasts: Analysis of the ECMWF Operational Forecasting System. Weather Forecast. 23, 1032–1043. https://doi.org/10.1175/2008WAF2222126.1.

WMO, 2018. Guide to Instruments and Methods of Observation Volume I – Measurement of Meteorological Variables. 2018 edition. WMO No. 8.

This is a post-peer-review, pre-copyedit version of an article published in *Agricultural Water Management*.
The final authenticated version is available online at: *https://doi.org/10.1016/j.agwat.2021.107169*